

**DESIGN OF SMALL TAG ANTENNA  
FOR EMBEDDED RFID TRACKING  
SYSTEM**

**KOH HAO ZHE**

**UNIVERSITI TUNKU ABDUL RAHMAN**

**DESIGN OF SMALL TAG ANTENNA FOR EMBEDDED RFID  
TRACKING SYSTEM**

**KOH HAO ZHE**

**A project report submitted in partial fulfilment of the  
requirements for the award of Bachelor of Electrical and Electronic  
Engineering with Honours**

**Lee Kong Chian Faculty of Engineering and Science  
Universiti Tunku Abdul Rahman**

**April 2023**

**DECLARATION**

I hereby declare that this project report is based on my original work except for citations and quotations which have been duly acknowledged. I also declare that it has not been previously and concurrently submitted for any other degree or award at UTAR or other institutions.

Signature :



Name : Koh Hao Zhe

ID No. : 1803327

Date : 25/4/2023

**APPROVAL FOR SUBMISSION**

I certify that this project report entitled “**Design of Small Tag Antenna for Embedded RFID Tracking System.**” was prepared by **Koh Hao Zhe** has met the required standard for submission in partial fulfilment of the requirements for the award of Bachelor of Engineering (Honours) Electrical and Electronic Engineering at Universiti Tunku Abdul Rahman.

Approved by,

Signature :   
\_\_\_\_\_

Supervisor : Dr Lee Yong Hong  
\_\_\_\_\_

Date : 18/05/2023  
\_\_\_\_\_

Signature :   
\_\_\_\_\_

Co-Supervisor : Prof. Ts. Dr. Lim Eng Hock  
\_\_\_\_\_

Date : 21/05/2023  
\_\_\_\_\_

The copyright of this report belongs to the author under the terms of the copyright Act 1987 as qualified by Intellectual Property Policy of Universiti Tunku Abdul Rahman. Due acknowledgement shall always be made of the use of any material contained in, or derived from, this report.

© 2023, Koh Hao Zhe. All right reserved.

## ABSTRACT

A novel miniature Radio Identification (RFID) tag antenna has been proposed for embedded metal tracking applications. It uses the meander and shorting techniques to achieve miniaturization, causing the overall antenna size ( $30 \times 30 \times 3.2 \text{ mm}^3$ ) to be much smaller than other contemporary tag antennas. The incorporated meandered lines and shorted stubs supply additional inductive reactance to the antenna impedance to cancel the capacitive impedance of the UCode8. Despite its compact size, the tag antenna can generate a strong directional radiation when it is embedded inside a metal, which is hardly achieved by conventional metal tag antennas. Prototypes are fabricated and they are tested in a controlled environment in the anechoic cabinet using industrial standard RFID testing equipment and software tools. It has been found that the proposed tag antenna can generate directional radiation patterns with a realized gain up to 0.337 dB when it is placed on a metal plate embedded in a metal cavity. At resonant frequency of 926 MHz, the impedance matching level is almost 100% with an achievable read distance up to ~18.88 m when the tag antenna is either embedded in metal or tagged on metal surfaces. Measurement results show that, the proposed antenna is highly versatile in tracking applications, as it can be embedded in or on metal without significantly affecting its performance.

## TABLE OF CONTENTS

<b>DECLARATION</b>	<b>i</b>
<b>APPROVAL FOR SUBMISSION</b>	<b>ii</b>
<b>TABLE OF CONTENTS</b>	<b>v</b>
<b>LIST OF TABLES</b>	<b>vii</b>
<b>LIST OF FIGURES</b>	<b>viii</b>
<b>LIST OF SYMBOLS / ABBREVIATIONS</b>	<b>xi</b>
<b>LIST OF APPENDICES</b>	<b>xii</b>
<b>CHAPTER</b>	
<b>INTRODUCTION</b>	<b>1</b>
1.1    General Introduction	1
1.2    Importance of study	6
1.3    Problem Statement	7
1.4    Aim and Objectives	7
1.5    Scope and Limitation of the Study	8
<b>LITERATURE REVIEW</b>	<b>10</b>
2.1    Overview	10
2.2    Coupled-PILA for Miniature On metal RFID Tag Design	10
2.3    A Compact Spiral-Shaped Loop Fed with high Read Range Tag Antenna for UHF RFID Applications	12
2.4    Compact Planar Inverted-S Antenna With Embedded Tuning Arm for On-Metal UHF RFID Tag Design	14
2.5    Folded Compact C-Shaped Antenna for Metal-Mountable RFID Applications	15
2.6    Summary	16
<b>METHODOLOGY AND WORK PLAN</b>	<b>18</b>
3.1    Overview	18
3.2.1    Project Overview	19
3.2.2    Project planning	20
3.2.3    Determined type of antenna	24
3.2.4    CST simulations	25

3.2.5	Analyse data obtained from CST	26
3.2.6	Optimization process.	27
3.2.7	Mask Making	28
3.2.8	Etching	29
3.2.9	Measurement	37
3.3	Summary	41
<b>RESULTS AND DISCUSSION</b>		<b>42</b>
4.1	Introduction	42
4.2.1	Result	43
4.2.2	Meandered Line Width Parametric analysis	47
4.2.3	Metal Cavity Depth Parametric Analysis	50
4.2.4	Metal Cavity Size Parametric Analysis	52
4.3	Prototype Measurement	55
4.4	Result Summary	60
<b>CONCLUSION AND RECOMMENDATIONS</b>		<b>64</b>
5.1	Conclusion.	64
5.2	Recommendations for Future Works	65
<b>REFERENCES</b>		<b>66</b>
<b>APPENDIX A</b>		<b>68</b>

**LIST OF TABLES**

Table 1.1:	Differences between the barcode systems and the RFID systems.	5
Table 3.1:	Project planning	22
Table 4.1:	The comparison of UHF RFID with miniature metal mountable properties.	62

## LIST OF FIGURES

Figure 1.1: RFID tag use for cashless toll transaction.	2
Figure 1.2: RFID system configuration	3
Figure 2.1: The coupled-PILA miniature RFID antenna	11
Figure 2.2: the RFID tag antenna geometry	12
Figure 2.3: The Equivalent circuit of antenna with spiral shaped feed	13
Figure 2.4: PISA with embedded u-shaped arm antenna	14
Figure 2.5: Compact folded C- shaped antenna. (Lee et al.,2019)	16
Figure 3.1: Flow chart of project	19
Figure 3.2: Waveguide dimension	24
Figure 3.3: Mesh view of the simulation	26
Figure 3.4: Parameter sweep of one of the design	28
Figure 3.5: Mask drawing in CST Simulation	28
Figure 3.6: Printed Mask	29
Figure 3.7: Cutting Photoresist to desired size	29
Figure 3.8: Laminated copper sheet with photoresist film.	30
Figure 3.9: The exposed photoresist immersed in developer solution.	31
Figure 3.10: Dissolved photoresist	31
Figure 3.11: The copper sheet put inside the boiling machine	32
Figure 3.12: The copper etched sheet	33
Figure 3.13: Photoresist layer dissolve in NaOH solution	33
Figure 3.14 Completed RFID antenna.	34
Figure 3.15: Styrofoam paste to the back of the antenna	35
Figure 3.16: Back of the RFID antenna	35

Figure 3.17: Commercial UHF RFID tags	36
Figure 3.18: Extracted Ucode8 Chips	36
Figure 3.19: Completed RFID Tag	37
Figure 3.20: The measurement setup to obtain the read distance pattern across all the three different planes.	39
Figure 3.21: Calibration of the Tagformance system	39
Figure 3.22: x-y plane measurement in anechoic chamber	40
Figure 3.23: x-z plane measurement in anechoic chamber	40
Figure 3.24: y-z plane measurement in anechoic chamber	41
Figure 4.1: Top and side views of the proposed antenna	43
Figure 4.2: The simulated $S_{11}$ (Impedance matching) when RFID tags on the metal plate	44
Figure 4.3: Z parameter of the RFID tags on metal plate.	45
Figure 4.4: The simulated $S_{11}$ (Impedance matching) when RFID tags embedded in metal plate.	46
Figure 4.5: Z parameter of the RFID tags embedded in metal plate.	46
Figure 4.6: Parametric analysis of the S-parameter on the width of the meandered strip	49
Figure 4.7: Parametric analysis of the Z-parameter on the width of the meandered strip	49
Figure 4.8: Linear realized gain when Depth =19mm	51
Figure 4.9: Parametric analysis of the Read Range with increasing embedded metal depth, d	51
Figure 4.10: Parametric analysis of the Realized Gain (dBm) with increasing embedded metal depth, d	52
Figure 4.11: Linear realized gain when cavity size, w =50mm	53
Figure 4.12: Linear realized gain when cavity size, w =170mm	53
Figure 4.13: Parametric analysis of the Realized Gain (dBm) with increasing embedded metal cavity size, w	54

Figure 4.14: Parametric analysis of the read range with increasing embedded metal cavity size, $w$	54
Figure 4.15: x-y plane Read Range of RFID Prototype between In metal and On metal measurement	55
Figure 4.16: x-y plane Polar Read Range of RFID Prototype between In metal and On metal measurement	56
Figure 4.17: x-z plane Read Range of RFID Prototype between In metal and On metal measurement	57
Figure 4.18: x-z plane Polar Read Range of RFID Prototype between In metal and On metal measurement	58
Figure 4.19: y-z plane Read Range of RFID Prototype between In metal and On metal measurement	59
Figure 4.20: y-z plane Polar Read Range of RFID Prototype between In metal and On metal measurement	60

**LIST OF SYMBOLS / ABBREVIATIONS**

$\Omega$	electrical resistance
$\epsilon_r$	relative permittivity
$\mu_r$	relative permeability

**LIST OF APPENDICES**

Appendix A : U code 8 datasheet

67

## CHAPTER 1

### INTRODUCTION

#### 1.1 General Introduction

The idea of radio waves being reflected for communication has been around for a very long time and predates radar technology. Radio communication technology underwent a significant development in the early 20th century and became widely employed in military drills to communicate with allies and spy on enemies. For example, in World War II, the allies employed the British-developed Identify-Friend or Foe (IFF) transponder to distinguish between friendly and enemy aircraft. (Ha & Chawla, 2007). The scientific community's interest in RFID was particularly notable in the 1960s and 1970s. A passive RFID transponder that could couple and rectify energy from an interrogator's electromagnetic field and send messages at a harmonic of the received frequency was created and patented by Richardson in July 1963.

The first commercial applications of RFID appeared in the start of the 1960s. To prevent item theft, Sensormatic and Checkpoint were formed and developed electronic article surveillance (EAS) technology. These systems only employ 1-bit tags, which can only register the values 1 and 0. However, the tags are affordable and offered excellent anti-theft protection (Landt, 2005).

The United States government began developing RFID systems in the 1970s, and Los Alamos National Laboratory was ordered to create a system for commercial usage, particularly in the application of tracking nuclear stockpiles. The scientists recommended installing an RFID reader at the security gate and attaching the RFID tag to the vehicle during the improvement of the RFID. The reader is able to recognise the related tag's recognition data and validate it as though electromagnetic waves were propagating from the reader to the tag and then backscattered to the reader. In 1980, the first systems for cashless toll transaction were starting to use the working concept of the RFID system. In Malaysia, where the government just began incorporating an RFID technique into the toll across the country to achieve cashless transaction systems, this type of cashless toll transaction system is extremely widespread. By the end of

2022, the government hopes to have 60% of tolls collected using RFID, and by the end of 2023, it plans to discontinue using Touch 'n Go (TnG) and SmartTAG cards altogether.



*Figure 1.1: RFID tag use for cashless toll transaction.*

As part of Industry Revolution 4.0, radiofrequency identification devices (RFID) are becoming more important technological tools in the manufacturing and logistics sectors. The integration of the manufacturing and network connectivity sectors into an Internet of Things is one of the promises of the fourth industrial revolution, according to Murofushi and Tavares (2017). Intelligent information and communication technology, or ICT-based machines, systems, and networks, are proficient at independently exchanging and responding to information and data to manage industrial production processes, and smart production and logistics have become the standard in this industrial world. The IoT revolution is driving a major advancement and revolution in UHF (RFID) technology, which is causing a wide-spread dispersion of various passive RFID tag types in items based on (Bahr & Price, no date).

When an RFID tag is exposed to UHF radio waves at the chosen frequency and with the proper communications protocols from an RFID reader, data is broadcast from or written to the tag using a microchip. Radio Frequency Identification, or RFID, is the abbreviation. It is a technology that uses radio waves to transport coded information sets, as the name would imply. RFID readers is a interrogator that receive a radio signal from the reader which then communicate the data to the RFID tags, which also known as transponders. The tag is turned on, and the reader receives the

data. The gathered data is sent to RFID middleware for processing so that it can be used in business applications. Each tag contains specific identification data, such as the manufacture date, shipping information, item ID, expiration date, etc., regarding the object to which it is attached. RFID tags come in two varieties: active (battery-powered and actively transmitting a locating signal) and passive (powered by electrical and magnetic energy received from the RFID reader).

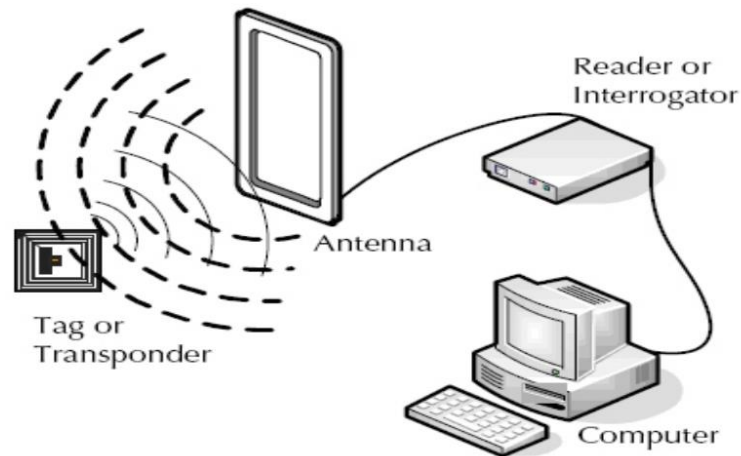


*Figure 1.2: RFID system configuration*

Supply chain and logistics management are among the sectors that have benefited the most from RFID technology. The domains where RFID has been employed in supply chains typically include logistics and transportation, assembly and manufacturing, asset identification and tracking, location monitoring, and environmental conditions (Hamadeneg, 2021). As operational efficiency in the logistics warehouse refers to accomplishing daily activities with the least amount of money, time, and labour, RFID can boost operational efficiency in the warehouse. RFID can help users grab orders from the correct shelves in the shortest time possible by identifying and locating the orders with the aid of RFID chips as picking operations is one of the most difficult and complex tasks in a warehouse. RFID can also reduce the work done and make the job easier for staff warehouses and managers.

Additionally, the supply chain's efficiency can be improved because the parcel can be easily scanned and identified without needing to be in the line of sight thanks to RFID's better reading rate and superior reading range. Therefore, RFID can

minimise labour and minimize the amount of time it takes to identify a package during both its import and its export.

*Table 1.1: Differences between the barcode systems and the RFID systems.*

<b>Characteristics</b>	<b>RFID</b>	<b>Barcode</b>
<b>Rate of reading</b>	RFID can be scanned multiple tags at once, fast reading.	Need to scan each tag individually, slow reading
<b>Information identification</b>	RFID allows multiple tag identification.	Single tag identification
<b>Robustness and reusability</b>	RFID can be made with waterproof material. Sturdier and more reusable.	Barcode tags are printed on paper or adhesive and are more susceptible to damage.
<b>Reading capability and reading range</b>	Do not need to be in the line of sight for tag reading. Reading range up to 15 meters	Scanner needs to be in line of sight with the tag, which results in short reading range
<b>Data size</b>	RFID tags have a greater capacity for complex data storage.	limited amount of data
<b>Information configuration</b>	Encoded with read and write functionality.	Read-only functionality

The table above illustrates the distinctions between barcodes and RFID by making reference to Table 1.1. (White et al., 2007). In comparison to the barcode system, the RFID has a higher reading rate, numerous tag identifications, is more durable and reusable, has a better scanning capacity and range, can store larger data

sizes, and has better functionality. However, the most significant disadvantage of RFID is its higher cost as compared to the barcode technology.

A tag that is embedded in an object rather than being attached to its surface is known as an embedded RFID tag. The advantage of employing embedded passive RFID over typical surface-sticking RFID is that the tag is very difficult to fake or remove because it is a part of the product. The tag cannot be taken off without also removing some of the device's parts. Because of this, integrated RFID effectively prevents theft.

Additionally, embedded tags are shielded from environmental threats including abrasion, chemicals, and other hazards of the environment where the item they are embedded in is used. Given the age and fragility of the glue, the RFID will continue to function and be safe from drops and damage. As a result, embedded RFID is more reliable than traditional RFID.

## **1.2 Importance of study**

Embedded RFID tags provide more protection to fragile RFID tags in harsh environments as the tag is secure inside compared to a surface RFID, where the tag has a risk of being damaged and being knocked off the surface. However, the current market of embedded RFID has a lower read range because the radiating wave cannot penetrate through the embedded metal.

Besides, the cost of the RFID, which is hundreds of times more than a barcode system, is the drawback of the existing embedded RFID. The price of standard RFID tags varies on their type and quantity. According to (Sheffield, no date), the setup costs for configuring the system with the required tag reader are a drawback of RFID. A barcode has a lower recurring price than RFID, which is another difference. As a result, creating a smaller RFID can lower the cost of the RFID by reducing the amount of material used for the RFID and making it simpler to incorporate into the product, resulting in a better-linked IoT system.

Hence, this study's findings could significantly impact the embedded tracking system's ability to get more excellent far-field performance out of the compact UHF bandwidth RFID tag antenna while maintaining a small size and simple structure.

Developing a small-scale UHF RFID tag antenna with high-performance far-field gain for embedded metal-mountable applications will mark a significant turning point in wireless communications technology by providing uncompromised long-read range RFID identification in the embedded application for more secure and protection compared to surface RFID tags. Additionally, the RFID's straightforward and simple structure can help lower the technology's cost, making it a more cost-effective option for use in the market.

### **1.3 Problem Statement**

An ideal UHF RFID tag antenna has several characteristics, including an operating frequency in the UHF bandwidth, which spans 902-928MHz, high impedance matching level, high radiation efficiency, small antenna size, and high far-field gain with a long read range of up to 12m.

However, when designing a new type of RFID tag antenna, numerous problems must be resolved. The radiation performance of the tag antenna can deteriorate, and the antenna resonant frequency can detune when the tag antenna is brought closer to the conductive platform. The degradation is amplified when the tag antenna is embedded in a recessed cavity. To prevent the RFID tag antenna from coming into contact with conductive material, spacer sheets of various materials, such as PVC, can be inserted into the antenna and inspired by the designs of folded patch antennas (Meng, Ma, and Zhao, 2022). However, using spacer can potentially increase the fabrication cost and reduce the antenna's robustness.

To date, only a few existing on-metal UHF RFID tag antennas are capable of producing good read range when embedded into metallic cavities. These tag antennas are bulky in size and have complicated structure, making them impractical for commercial use.

### **1.4 Aim and Objectives**

The purpose of the project is to develop a miniature UHF RFID tag antenna for a tracking metallic object. The tag antenna can be attached directly on metal or embedded in metallic cavity. This antenna can cover the entire UHF spectrum space..

Additionally, the tag antenna's overall size must be kept as small, tiny and compact as possible while adhering to the previous requirements.

The objectives of the project are:

- To design a small tag antenna, less than 40 mm × 40 mm, whose resonance frequency is located within the regulated UHF passband, 902 MHz – 928 MHz.
- To tune the tag antenna's input impedance to achieve conjugate match with the chip impedance.
- To achieve a maximum far-field gain of no less than -3 dB and a peak read range of more than 10 m when the tag antenna is attached on metal or embedded in a metallic cavity.

### **1.5 Scope and Limitation of the Study**

This project is to design a small RFID tag antenna for embedded tracking system using the commercial 3-D simulating software, CST Studio Suite 2021. This software will be used to perform a simulation of the RFID tag antenna to study its resonant working frequency, bandwidth of the antenna, impedance matching, far-field gain, energy efficiency antenna, radiation efficiency, far field patterns, etc. After the simulation, the antenna prototypes will be fabricated using the conventional PCB etching method. The process starts with combining copper foil with polyester PET plastic film, then treating the surface of the combined composite copper foil with an etching solution. The Voyantic Tagformance system will be used to evaluate the read range and tag sensitivity of the antenna prototypes.

The project scope does not include the design and program of the RFID microchip. Instead, the tag antennas use the UCODE 8 microchips, which are sourced from NXP Semiconductors. Besides, the project scope does not include the finding of an external company to manufacture the proposed RFID tag antennas on a large scale. The project's only goal is to make a prototype to test how well the antenna works.

The limitation of the research is that the university lacks industry-level infrastructure with good PCB etching technology. The current PCB etching facility may have a small level of inaccuracy. As a result, it is very challenging for designing

antenna that has a long and narrow slits design. Besides, due to incomplete infrastructure to produce the antenna prototypes, some processes must be done manually. Hence, this causes the possibility of human error, which will further impact the inaccuracy of the antenna and yield differences between simulated and measured results of the antenna performance.

## CHAPTER 2

### LITERATURE REVIEW

#### 2.1 Overview

This study aims to suggest a novel technical design for a miniature UHF RFID compact tag antenna that can be used in an embedded tracking system. The antenna's footprint is the primary determinant of the tag's dimensions while creating a small RFID. Other miniaturization techniques have been suggested to reduce the tag size, including high-permittivity substrates, etched slots, and meandering radiators. Thus, numerous pieces of literature are being reviewed to learn and understand the techniques and knowledge behind designing RFID tags so that a high-performance miniature UHF RFID tag antenna can be fabricated.

#### 2.2 Coupled-PILA for Miniature On metal RFID Tag Design

According to Lee et al. (2020), the design can combine two planar-inverted L-antennas (PILA), which serve as radiators and couplers individually, to generate a small RFID tag. By magnetically coupling a PILA to the radiator, directed currents are produced to achieve miniaturization. Since physically meandering, the radiator does not produce meandering currents. Therefore, the antenna can be made electrically small without noticeably affecting read distance and radiation efficiency. It is almost impossible to achieve traditional meandering structures' efficiency.

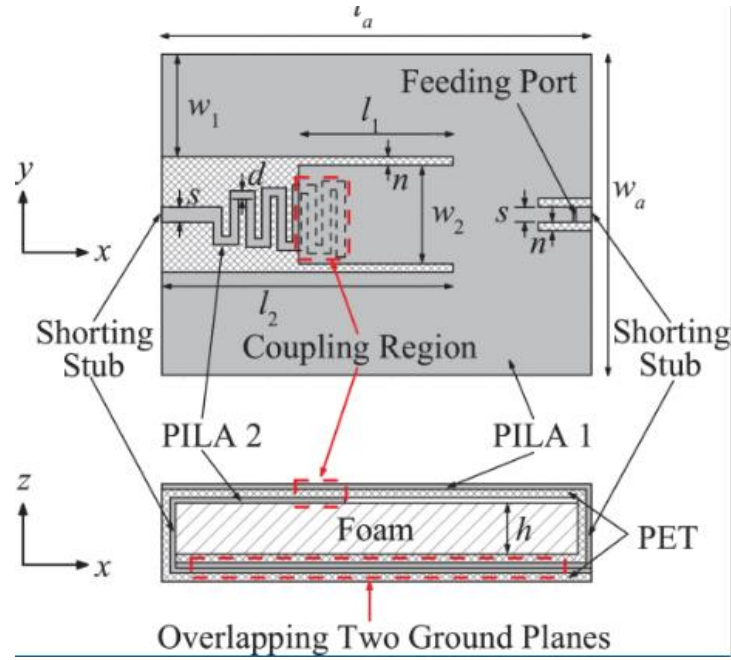


Figure 2.1: The coupled-PILA miniature RFID antenna

The reviewed journal's RFID antenna has a structure size of  $25\text{mm} \times 18.75\text{mm}$  with a total antenna area size of  $468.75\text{ mm}^2$ . The proposed antenna comprises two simple coupled planar inverted-L antennas. The PILA number 1, functioning as the radiator in this design, is shorted to the ground via a thin stub at the antenna end of its radiating patch. Moreover, to further enhance the tuning range of the input reactance, the two notches around the stub are opened up. Successively, PILA 1 is magnetically coupled to PILA 2 at the other end of its radiating patch. As a result, increasing the current density improves the antenna's far field gain.

The result obtained from the reviewed journal is found to have a input impedance of  $7.45 + j191.19\ \Omega$  with the resonant frequency of 915 MHz, where it has a very high impedance matching with the chip impedance  $13 - j191\ \Omega$ .

### 2.3 A Compact Spiral-Shaped Loop Fed with high Read Range Tag Antenna for UHF RFID Applications

Bansal et al. (2019) claimed that using a meandering structure can minimize the size of the RFID antenna since it boosts electrical length while reducing the size of the physical structure. RFID tag antennas also use inductively coupled feed and T-match stubs to achieve balanced inductance and eliminate the capacitive reactance in the chip impedance.

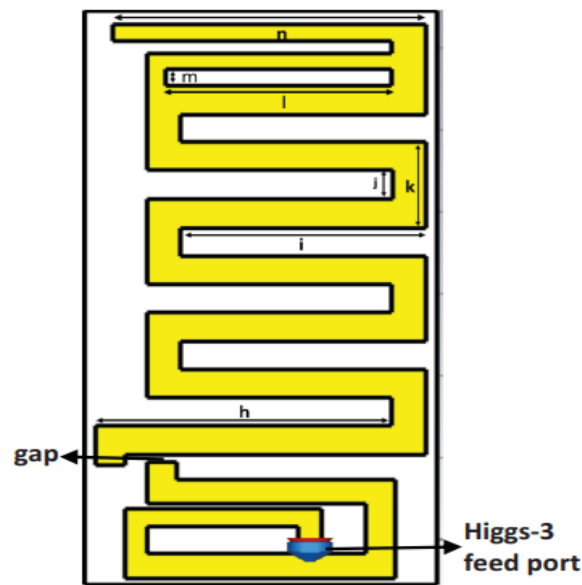


*Figure 2.2: the RFID tag antenna geometry*

From the journal, the RFID tag antenna features a meandering structure and a corresponding spiral-shaped loop printed on Roger substrate RO4350 with a height of 0.8 mm and a dielectric constant of 3.3, according to the examined publications. The proposed tag structure's impedance is also calibrated and set to achieve resonance in the European RFID Band (865-867 MHz). Figure 2.2 shows the planned antenna's dimensions, which are 68 x 34 x 0.8 mm<sup>3</sup>. Compact, with a volumetric size of 1849 mm<sup>3</sup> and a gain of 2.23 dB, is the suggested meandering antenna.

According to the peer-reviewed journal, the radiating element length, meandered strip width, and gap between meandered turns are all investigated and optimized to reach resonance in the UHF region at 866 MHz while preserving the antenna's good performance.

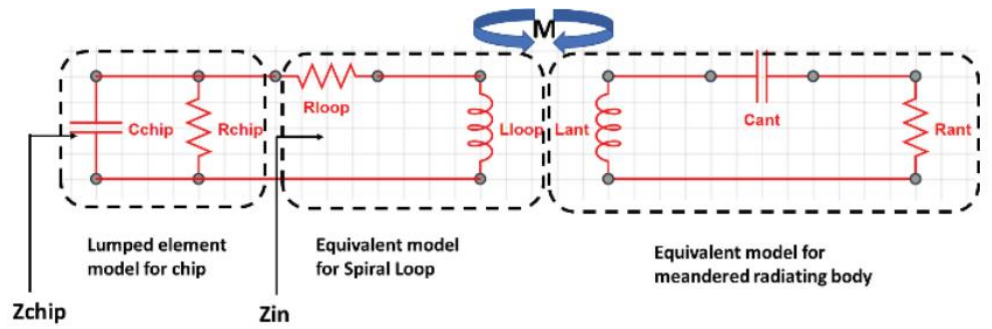


Figure 2.3: The Equivalent circuit of antenna with spiral shaped feed

Changing the loop width and height specifications may determine the reactance  $X_{in}$ . On the other hand, by adjusting the distance between two elements, the resistance of the antenna can be determined.

$Z_{loop} = R_{loop} + j X_{loop}$ , which converts the impedance of the radiating antenna, can be modelled as an impedance transformer as seen in figure 2.3,  $Z_{ant} = R_{ant} + j X_{ant}$  is used to match the chip impedance, which can be defined as  $Z_{chip} = R_{chip} + j X_{chip}$ . Additionally,  $Z_{in}$  is the tag antenna's overall input impedance as measured at the feeding end of the tag antenna.  $M$  also denotes the degree of connection between the spiral loop and the radiating element, which maximizes power transfer to the chip. The chip impedance must be conjugated with the impedance of the tag antenna  $Z_{in}$ .

The simulated results of the return loss of the designed tag antenna considering the lumped element value of the chip impedance has a return loss of -36 dB is observed at the centre frequency of 866 MHz. Next, the maximum gain from the spiral-shaped loop fed antenna at 866 MHz is 2.21 dB.

To wrap up this article, an RFID tag antenna with the dimensions 68 x 34 x 0.8 mm<sup>3</sup> that consists of a spiral-shaped inductively coupled matching loop configuration and a meandering radiating element is built. Even though the designed tag antenna uses the meandered line structure, which is a current dissipating structure that will reduce the far-field gain of the antenna, the designed antenna still has a simulated gain of 2.62 dB. This is due to the large width of the meandered line and meandered gap, which is 2 mm. Thus, using larger meandered lines and gaps, the

antenna's electrical waveguide length can be increased without sacrificing the RFID antenna's far-field gain and read range. However, this design has a massive antenna size of  $68 \times 34 \text{ mm}^2$ , which cannot be used for compact RFID-embedded application.

## 2.4 Compact Planar Inverted-S Antenna With Embedded Tuning Arm for On-Metal UHF RFID Tag Design

Ng et al. (2019) state that a folded patch, which is semiflexible because the antenna structures are designed on a flexible wafer-thin film, has recently been suggested for designing several low-cost and small-sized tag antennas. This is because the antenna structures are then folded around a dielectric soft foam. However, a meandered slot line or a large number of slots must be incorporated into the tag design in order to create a high-performance folded patch. This decreases the resistance and reactance of the folded-patch antenna and causes them to have poor impedance matching because there isn't enough resistance to conjugate with the chip impedance.

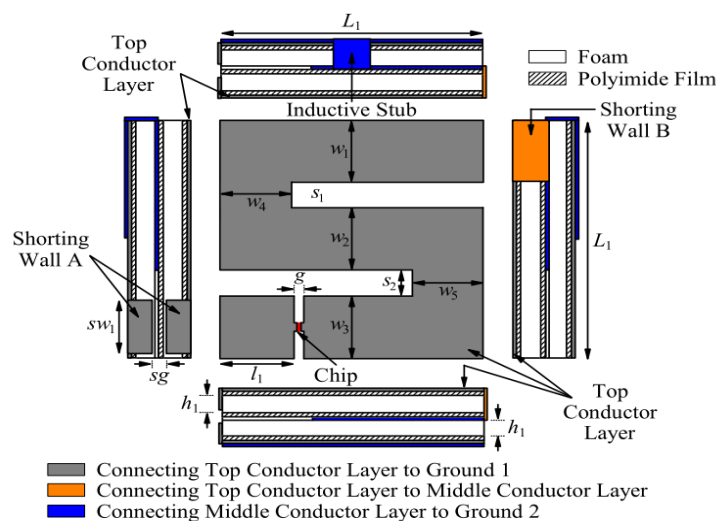


Figure 2.4: PISA with embedded u-shaped arm antenna

Figure 2.4 demonstrates that the serpentine patch and the U-shaped arm serve as current guides, and the areas with the highest current densities are found in and around these areas. In comparison, the serpentine patch's lower portion has modest current densities. Due to the presence of the U-shaped arm beneath the upper half, the current densities of the upper part are higher than those of the bottom part. This is

because the current density in this patch region increases due to the currents on the U-shaped arm induced by the currents on the upper half of the serpentine patch.

The antenna footprint size can be effectively decreased by having simply a 15 mm × 15 mm × 3.2 mm U-shaped arm with a serpentine patch. With a recorded maximum realized gain of 2.85 dB at 921 MHz. Besides, the antenna's power transmission coefficient between the tag and the antenna is greater than 90%, with the read distance that can be achieved when placed on a metallic object above 7 m and up to a maximum range of 11.9 m.

Despite having a relatively small footprint of 15mm x 15mm x 3.2mm, the RFID antenna from this study has a good maximum realized gain performance of -2.85 dB, and a maximum range of 11.9 m. However, because of the second layer PILA, production costs would soar because the double-layer design will significantly complicate the manufacturing and etching procedures.

## **2.5 Folded Compact C-Shaped Antenna for Metal-Mountable RFID Applications**

For on-metal applications, the paper presents a small antenna known as the compact folded C-shaped one in Figure 2.5. Several metal-mountable UHF tags have recently been investigated using a microstrip patch antenna. The antenna patch resonator, however, needs to be more significant to be used in tag antenna design due to its enormous footprint. By lowering the patch size by half and producing novel antenna topologies like the (PIFA) and planar inverted-L antenna (PILA), one side of the antenna radiator is shorted to the ground using metallic vias.

The loop antenna and the planar inverted-L antenna were combined to construct this antenna (PILA). This article's PILA structure combines with the loop antenna, which boosts radiation efficiency (Lee et al., 2019).

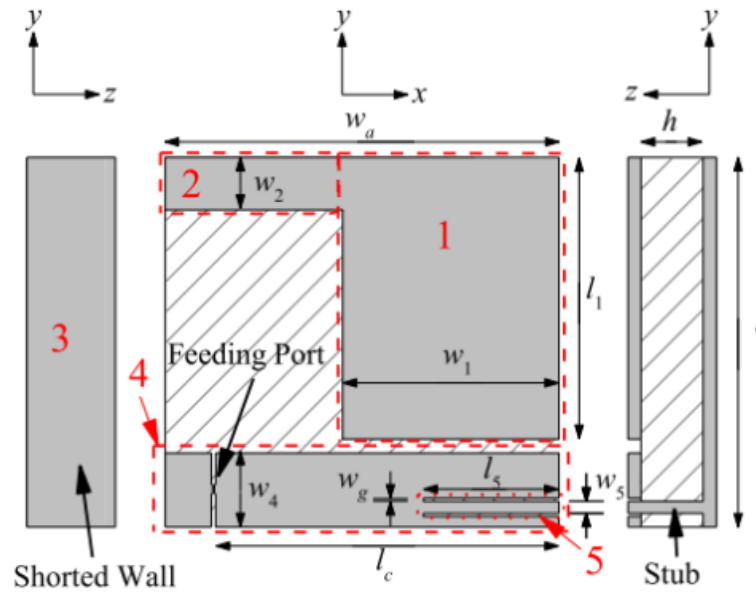


Figure 2.5: Compact folded C-shaped antenna. (Lee et al.,2019)

When placed on a metallic surface, the small C-shaped antenna radiates in a specific direction and has a realized gain of about 3.77 dB at the resonance frequency of 915 MHz. The simplicity of the structure and ease of fabrication make this antenna design effective. As a result, it is less expensive than other antennas. The antenna's loop structure in this study is extended with a parallel cut section of the inductive slime stub compared to the conventional loop antenna. The outcome indicates that a stronger magnetic field surrounds this stub, enhancing the small antenna's inductance. This on-metal tag antenna design has improved and solved the issue of image current degradation. The disadvantage of this antenna design is that it has a comparatively large construction compared to the other antenna structures stated earlier. The antenna is 40x40 mm and has a respectable realized gain of 3.77 dB. In addition, it can only generate a directed radiation pattern, which is insufficient to cover the entire space.

## 2.6 Summary

To summarise the literature review, the meandering line structure is a current dissipating construction that will lessen the antenna's far field gain. However, one can increase the electrical wave path length without significantly reducing the RFID antenna's far-field gain and read range by using a wider meandered line and a meandering gap larger than 1 mm. Additionally, the antenna footprint area in the U-shaped arm with the serpentine patch can be almost doubled using double-layer PILA to enable current density to rise in this patch region. This successfully minimizes the

size of the antenna structure while maintaining a very high far-field gain. However, because of the second layer, PIFA is highly difficult to make and costs more in labour and materials. As a result, embedded micro-RFID antennae cannot use PIFA.

Additionally, a compact folded C-shaped antenna with an additional horizontal inductive stub exhibits a stronger magnetic field strength in the vicinity of this stub, increasing the compact antenna's inductance. The simplicity of the structure and ease of fabrication of this antenna design makes it practical for usage on metal. As a result, it is less expensive than other antennas. This on-metal tag antenna design has resolved the issue of image current degradation. The disadvantage of this antenna design is that it has a comparatively large construction compared to the other antenna structures stated earlier. The antenna is 40 mm x 40 mm x 1.6 mm and has a respectable realized gain of 3.77 dB. Full spatial coverage cannot be achieved with the tiny C-shaped antenna since it can only produce a directed radiation pattern.

It has been determined that the tiny antenna structure that is suggested for usage in embedded tracking applications uses a meandering line to increase the electrical pathway to lower the antenna's resonance frequency to a UHF bandwidth. Additionally, it is suggested that the meandering line have a thick line and a gap to lessen its current-dissipating qualities. Nevertheless, the antenna structure must be a single layer rather than a double layer to save manufacturing costs. It is suggested that the antenna has an additional horizontal part of improving the magnetic field intensity around the inductive stub. This raises the tiny antenna's inductance. Last but not least, it is suggested that the antenna have a straightforward design to prevent difficulties in fabrication and production, increasing the dependability and lowering the cost.

## CHAPTER 3

### METHODOLOGY AND WORK PLAN

#### 3.1 Overview

The research objective is to fabricate and design a miniature UHF RFID tag antenna with a good performance antenna with high impedance matching, high far-field gain for embedded metal-mountable applications. To achieve the research objective, the newly designed antenna characteristics and performance needed to be identified by using simulations and physical prototyping. The quantitative data from the simulations and physical experiments will be obtained and analysed during the research period. The primary data obtained and used in this research were those obtained from individual experimental and simulation data. The CST simulation studio 2021 will be used for simulation and data gathering to study and design the RFID antenna. The physical prototype built will be tested on the Tagfomance system to determine the real-prototype performance compared to the software simulations.

### 3.2.1 Project Overview

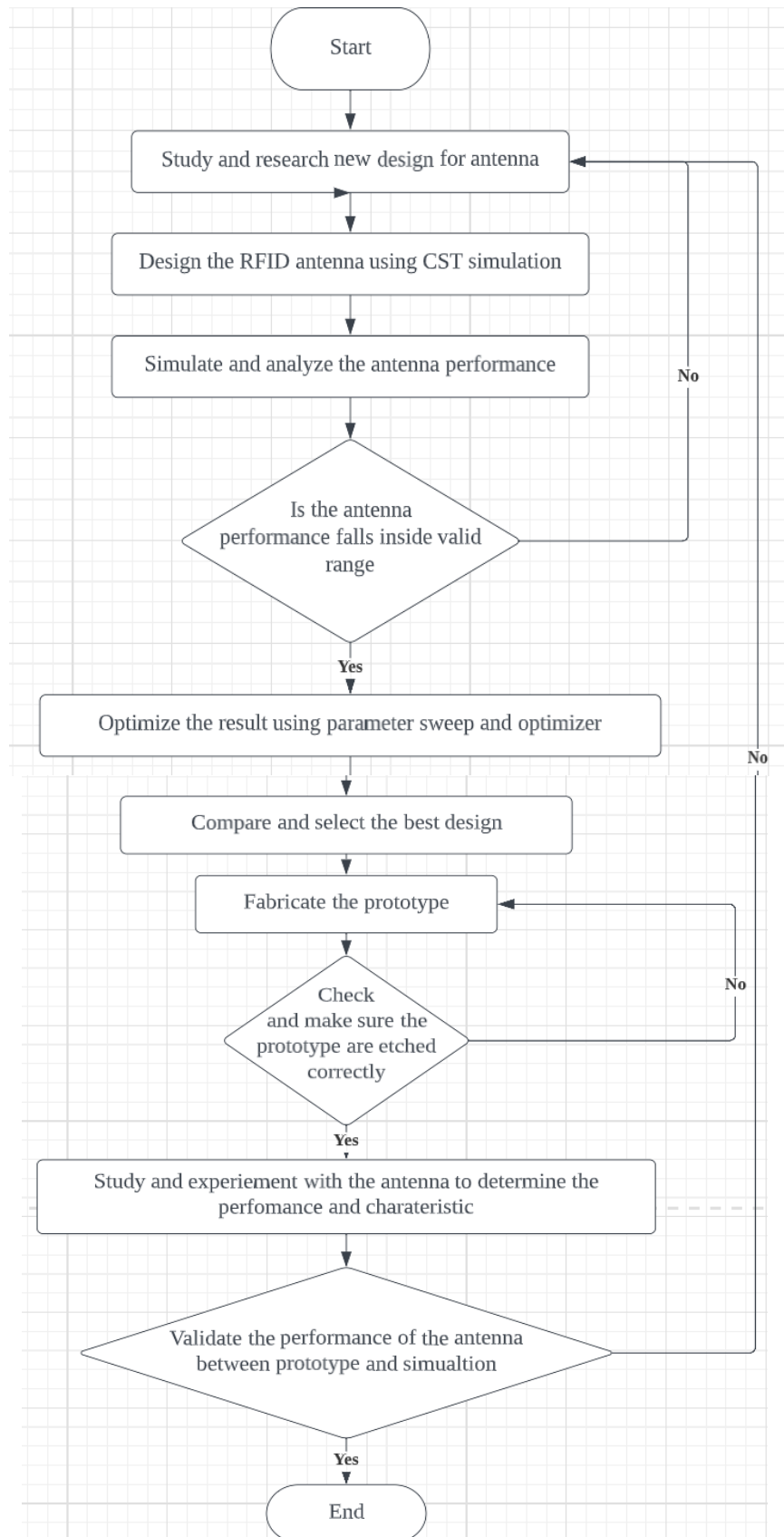


Figure 3.1: Flow chart of project

A brief overview of the project methodology can be explained in Figures 3.1. The project started with studying and researching the best way to design the antenna to accomplish the project objective. Next, the CST simulation will develop the desired RFID design. The design will then be stimulated and studied to understand the trend and characteristics of the antenna. If the simulated antenna performance and resonant frequency did not fall within an accepted range, a new design needed to be drawn. The optimization of the antenna will then follow by tweaking the antenna's dimension to optimize the antenna's far field gain, resonant frequency, and impedance matching. The project will then be followed by a comparison between multiple designed antennas to select the best design.

The finalized design will then be manufactured in a prototype etching process. The etched antenna will be checked to see if the process was done correctly and if all the dimensions were precisely etched. Next, the prototype will undergo experiments and testing to determine the antenna's performance. The result will be compared with the simulated result to validate the prototype result that functions in real-life conditions and is roughly the same as the simulated result.

### **3.2.2 Project planning**

Table 3.1 Presents the project's Gantt Chart, which outlines the development and planning of task for the project. The Gantt Chart was planned to understand the dependencies between the task and allow the project to be done within the given time frame.

The project task planning is divided into 3 stages. The first stage begins in June 2022 and concludes in September 2022, with tasks such as reviewing previous works for UHF RFID tags on miniature RFID topics, designing a miniature tag antenna, and analysing and optimising the electromagnetic model using the CST Microwave Studio.

The start of the second phase is The first process includes developing a theoretical model to investigate the tag antenna's radiation properties when used in an embedded system. The second and final steps involve creating prototypes of the ideal design between October 2022 and January 2023 after analysing the tag antenna's impedance properties.

The last phase of the project starts with the validation and measuring of the designed prototype to prove that the designed antenna has a miniature design and can be used in an embedded tracking system . On the other hand, the report-writing of the whole project is done throughout the project, from the first stages to the third phase to provide an efficient evaluation and obtain data

Table 3.1: Project planning

Part	Task	JUN	JUL	AUG	SEP	OCT	NOV	DEC	JAN	FEB	MAR	APR
		2022	2022	2022	2022	2022	2022	2022	2023	2023	2023	2023
1	Studying journal paper for UHF RFID tags regarding miniature RFID topics											
	Design miniature tag antenna CST Microwave Studio.											
	Simulate and optimize the antenna model using the parameter sweep.											
2	Design the antenna inside the embedded metal cavity to study the performance drop											
	Evaluate the characteristic of the tag antenna											
	Fabricate the antenna prototypes and validate the dimension of the physical antenna.											



### 3.2.3 Feeding Port

There are various of types of antennas can be used in the applications. However, for small size application, wave-guide source antenna or chip port source antenna was considered.

The wave-guide antenna size can be determined by using the formula below:

$$f_c = \frac{c}{\sqrt{\epsilon_r \mu_r}} \sqrt{\left(\frac{m}{2a}\right)^2 + \left(\frac{n}{2b}\right)^2}$$

Where  $c$  is the velocity of the light in vacuum with a value of  $2.9979 \times 10^8$ .  $\epsilon_r$  is the relative permittivity of the waveguide, and  $\mu_r$  is the relative permeability of the waveguide.  $B$  and  $m$  were the waveguide width and height, respectively, and  $m$  and  $n$  were the half-wave variations in the  $a$  and  $b$  directions, respectively. Thus, by getting an antenna to work in a UHF bandwidth ranging from 902 MHz to 928 MHz, the calculated result for  $a$  will be 247.65 mm and  $b$  is 123.825 mm. Thus, the large waveguide will need to have a very big antenna structure. Hence, the waveguide source antenna will not be well suited to the miniature embedded RFID applications. Hence, the chip source patch antenna was used in the design for the compact UHF RFID for embedded design applications.

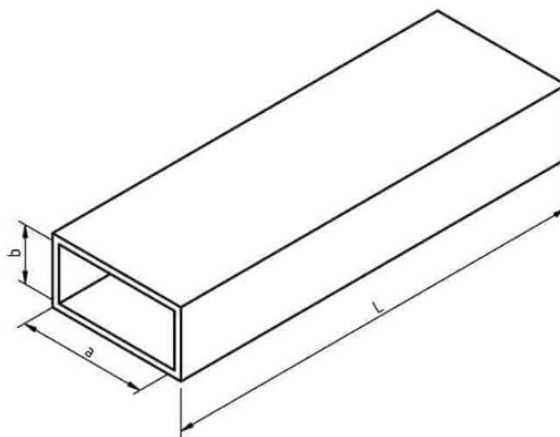


*Figure 3.2: Waveguide dimension*

### 3.2.4 CST simulations

The CST simulation Studio 2021 is chosen to be the simulation software used to design the RFID antenna and study the effect of the design on the characteristic of the RFID. The data that needed to be studied for the antenna's performance included the far-field gain, directivity, impedance matching, and resonant frequency.

The patch antenna with a microchip-sourced port is drawn with five layers, with the first layer being the copper that acts as the ground for the patch fixed at a thickness of 0.009mm, the same as the copper film used in the etching machine. The next level is polyethylene terephthalate, commonly known as PET, with a thickness of 0.025mm relative permittivity of 3. The dielectric constant is the permittivity of a material expressed as a ratio to the electric permittivity of a vacuum. The third material is the polystyrene foam substrate, with a fixed width of 3.2 mm and a relative permittivity of 1.06. The fourth level will be the second layer of the PET, and the fifth layer is the copper patch that will be etched to maximize the antenna's performance. The patch antenna has five layers due to the copper film used for the prototype, which comes with a support PET structure. The film is then wrapped around the foam dielectric substrate to form a patch antenna.

The simulation process starts by getting familiar with the basic operations of the application. The basic dipole structure is drawn by following the instructions from the Internet. However, the dipole antenna differs from the desired type of antenna, the microchip patch antenna. However, due to the simple structure of the antenna, which consists of only a simple tube, the simple structure can be quickly drawn and get familiar with the structure.

Next, the RFID patch antenna design from another journal design was drawn by following the parameters provided. By doing this, the simulated result can be reviewed and compared with the original journal's result to prove that all the steps and settings for the simulation were correct. If all the settings and steps are correct, the generated result should be roughly the same as the journal. Besides, the simulation setting was learned by setting up the mesh properties.

The so-called hexahedral mesh is the one that is utilized. The computational volume, which is the simulation space, including the RFID antenna model, is discretized using rectangular cuboids of varying sizes to create a hexahedral mesh. A

mesh cell is a name given to each cuboid. Figure 3.3 illustrates the view of a simulated mesh. The discretized representation of a small spatial region that makes up each mesh cell is used to compute the electric and magnetic fields. Naturally, as more mesh cells are used for discretization, the gradients in the area will be captured more accurately. However, the simulation time would be directly impacted by recklessly increasing the total number of mesh cells. Therefore, utilizing a mesh that offers a fair balance between simulation speed and outcome accuracy is crucial in the simulation of the RFID antenna.

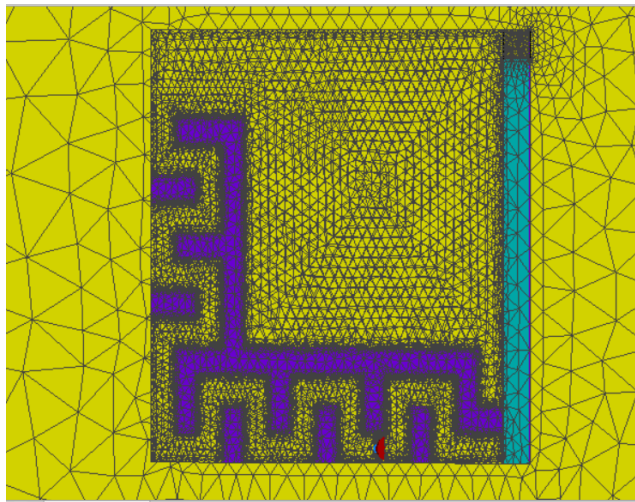


*Figure 3.3: Mesh view of the simulation*

### 3.2.5 Analyse data obtained from CST

The following method in designing a miniature embedded RFID is to study and discuss the impedance matching between the source and the antenna, the S-parameter, the resonant frequency of the antenna, input impedance which is the z-parameter, the far field gain, surface currents, and far-field radiation pattern and directivity obtained from the simulation. This chapter also looks at the proposed antenna's parametric analysis to determine its impedance and how well it can radiate.

The S-parameter was examined since a low S-parameter decibel demonstrated a good impedance match between the chip and the suggested antenna. The S-parameter graph's lower point also shows the tag antenna's resonance frequency. This is because the tag antenna is only resistive at 914 MHz, where the antenna's capacitance and inductance terminate each other and leave the purely resistive component.

Besides, the input impedance, known as the Z-parameter, is simulated and studied. If the imaginary Z-parameter. The proposed antenna uses the UCODE 8 microchip with a chip impedance of  $13 - j191 \Omega$ . So, during the resonant frequency, the Z-parameter must have a conjugate impedance to cancel out the chip impedance and get the best impedance matching and power transfer.

Besides, the radiation pattern and read distance were observed and analyzed. There are 2 types of radiation patterns: isotropic antennas that generate a radio wave field that propagates around the antenna, and highly directional antennas that concentrate the RF field in a specific direction. Besides, the performance of the antenna's far-field radiatively gain is the most crucial factor in RFID design. The higher the far field gain, the longer the read distance.

Furthermore, the surface current distribution inside the electrical pathway of the antenna is observed to understand the trend and pattern of the current flows. The surface current determines the high and low present density spots affecting the radiating patch. The distribution of the electrical and magnetic fields was observed and analysed in order to determine the polarisation of the radio wave and

### **3.2.6 Optimization process.**

The effects of the essential design parameters are therefore examined using parametric analysis, as seen in Figure 3.4. The impact of changing the width and length can be simulated multiple times by setting the number of samples needed to be sampled or setting the step width. Using the parameter sweep, the simulation time can be reduced by running all the possible values inside the ranges to study the trend and best parameters needed to obtain the optimized antenna. Besides, the local and global automatic optimization methods in CST Studio Suite are used to determine the optimizer parameter to achieve the best result. Local optimizers offer quick convergence but run the risk of convergent to a local minimum as opposed to the optimal overall solution, and global optimizers, on the other hand, search the entire problem space but often need more computations.

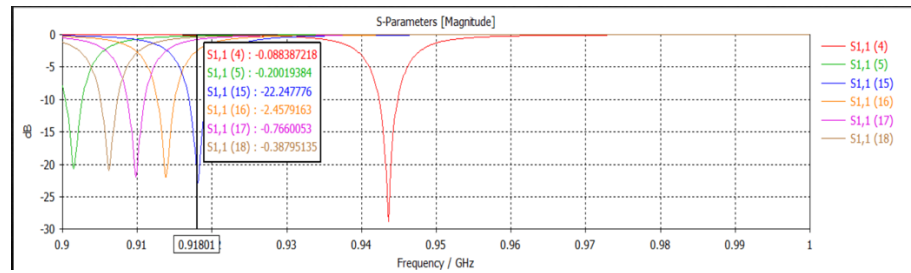


Figure 3.4: Parameter sweep of one of the design

### 3.2.7 Mask Making

The optimized antenna then varies in width, ranging from 1.8mm to 2.2 mm. This is because, during the prototype fabrication, the etching process may be imperfect and result in changes in the size of the fabricated RFID. Hence, the physical fabrication contains 5 different widths of the meandered line to ensure the fabricated antenna is the closest to the simulation due to human error in the etching process. The mask drawn in the CST simulation file can be seen in Figure 3.5.

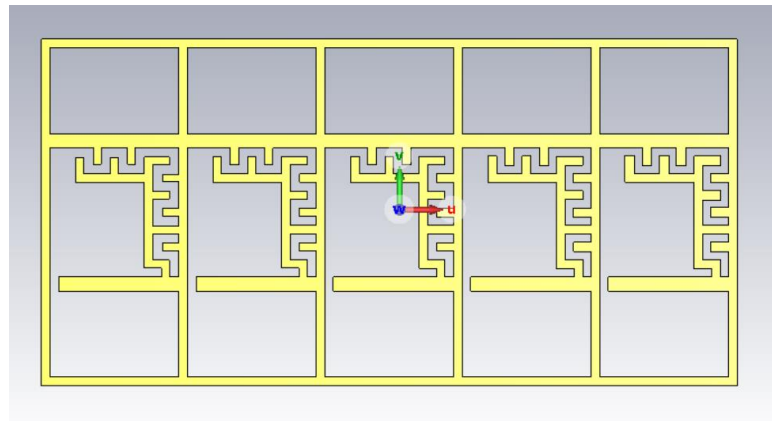
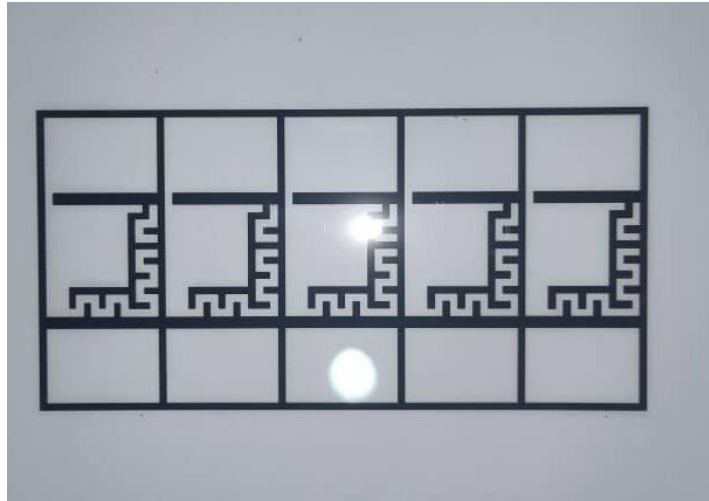


Figure 3.5: Mask drawing in CST Simulation

The CST drawing is then exported into the Aperture Template editor for further edits. Lastly, the edited template is then printed using the CircuitCam Software. The Mask is printed on polyester film, that can be referred in figure 3.6.



*Figure 3.6: Printed Mask*

### **3.2.8 Etching**

After the simulation, the prototype RFID will be produced using the etching method on the copper sheet. Firstly, the copper sheet is cut into the desired size that can accommodate 5 sets of RFID antennae. Next, the photoresist film is cut to cover the selected copper sheets in Figure 3.7. The photoresist used is the negative photoresist. The areas not exposed to light become more soluble in the developer solution. Next, the copper sheet and the cut photoresist are put onto the metal plate and go through lamination to laminate the photoresist together with the copper sheets, as seen in Figure 3.8. The lamination process is done carefully and slowly to ensure no air is trapped under the photoresist film to ensure the exposure to UV light can be done correctly in the upcoming steps.



*Figure 3.7: Cutting Photoresist to desired size*



*Figure 3.8: Laminated copper sheet with photoresist film.*

Next, the laminated copper sheet is placed in the UV exposure machine, and the printed mask is placed on the device. The photoresist film is exposed to light through a mask photomask containing the desired antenna pattern. As the photoresist film is the negative photoresist film, the light causes a chemical reaction in the photoresist film, which makes it insoluble in a developer solution. The pattern is then developed by selectively dissolving the exposed or unexposed areas of the photoresist film, leaving a patterned layer on the substrate. The exposed mask to the UV light is

then immersed in the etching solution to remove the unexposed part of the laminated photoresist, which can be referred to in Figure 3.9.



*Figure 3.9: The exposed photoresist immersed in developer solution.*

A strong alkaline chemical called "developer" is used to remove exposed photoresists. It selectively dissolves the photoresist that has not been exposed to light, leaving behind only the unexposed areas. The developer used in the etching solution is the sodium carbonate ( $\text{Na}_2\text{CO}_3$ ) solution. The dissolved photoresist can be referred to in Figure 3.10.

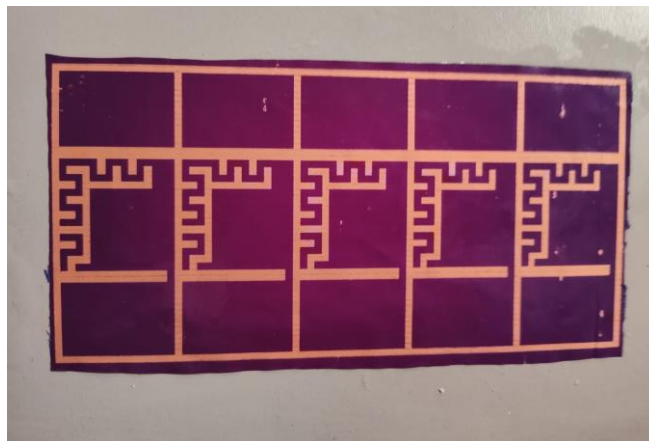


*Figure 3.10: Dissolved photoresist*

The dissolved photoresist is checked carefully to ensure the photoresist is covered perfectly without any holes and gaps. Human error may occur and let some air bubbles form during the lamination, causing the photoresist film to be not exposed to UV rays during the process and causing the layer to be dissolved by the developer during the dissolving process. Hence, masking tape is used to cover up the imperfection holes.

The covered photoresist copper sheet is then immersed in the copper etching solution. The copper etching solution is a chemical solution used to etch or remove copper from a copper substrate and leave the photoresist part where the photoresist film is a protective film to avoid the copper layer from being etched away. The copper etching solution is a mixture of hydrochloric acid (HCl) and hydrogen peroxide (H<sub>2</sub>O<sub>2</sub>) in a boiler machine, as shown in Figure 3.11. The copper sheet is then put inside the boiling machine for 10 minutes. The etched copper product can be seen in Figure 3.12

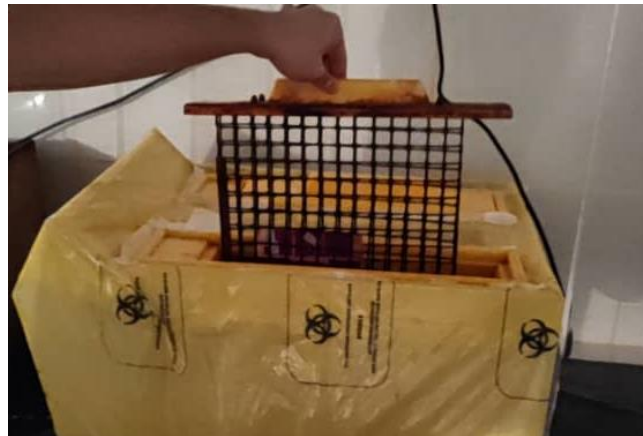


*Figure 3.11: The copper sheet put inside the boiling machine*

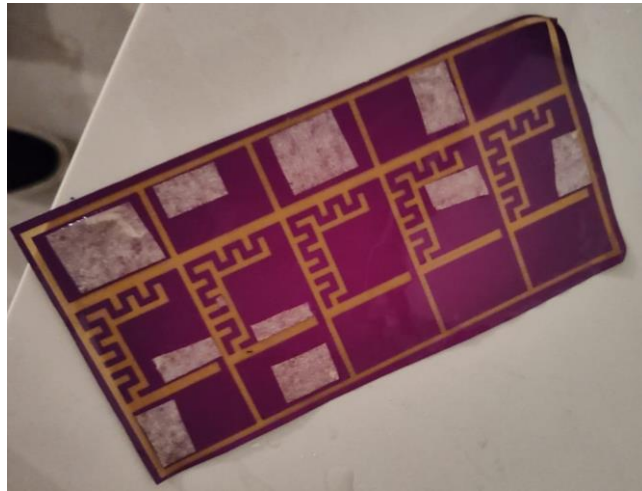


*Figure 3.12: The copper etched sheet*

Finally the etched copper sheet is immersed in sodium hydroxide solution (NaOH) to dissolve the remaining photoresist layer to exposed the copper layer as seen in Figure 3.13



*Figure 3.13: Photoresist layer dissolve in NaOH solution*

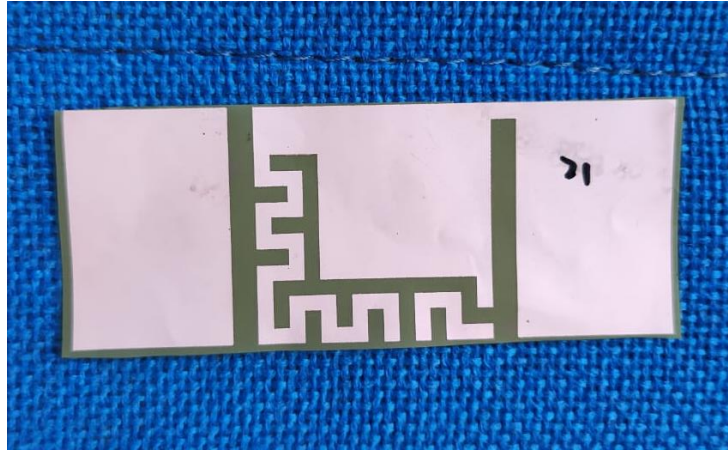


*Figure 3.14 Completed RFID antenna.*

After the etching process, the individual RFID antenna is cut for measurement, as seen in Figure 3.14. The double-sided tape is taped onto the back of the antenna, followed by sticking the Styrofoam on the back, as seen in Figure 3.15. The Styrofoam will act as the dielectric of the antenna. The reason for this is that the presence of a conductive ground plane beneath the antenna can interfere with the electromagnetic fields produced by the antenna, leading to reduced efficiency and accuracy in the RFID system. Introducing a dielectric material, such as Styrofoam, helps to improve the antenna's efficiency, as it allows the electromagnetic fields to propagate more efficiently between the antenna and the RFID tag. Styrofoam is a low-loss material that reduces the impact of the ground plane on the antenna by effectively raising the antenna above the plane and reducing the reflection and scattering of the electromagnetic waves at the ground plane. This improves the antenna's radiation pattern and enhances its ability to communicate with RFID tags. Finally, the ground is stuck and pasted together to enclose the antenna's ground fully. The back of the antenna can be seen in Figure 3.16.

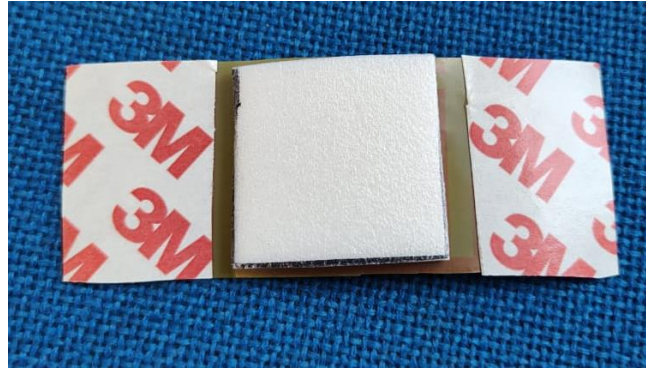


*Figure 3.15: Styrofoam paste to the back of the antenna*



*Figure 3.16: Back of the RFID antenna*

The next step is extracting the Ucode8 Chips from the existing commercial UHF RFID tags, which can refer in Figure 3.17. Extracting the Ucode8 Chips is far cheaper and faster than getting the Ucode8 embedded into the RFID antenna from a third party. The extraction of the Ucode8 chip is done by immersing it in water to remove the paper-like structure from the RFID tags. After removing the paper structure, the tags are cut and extracted carefully, as seen in Figure 3.18.



*Figure 3.17: Commercial UHF RFID tags*



*Figure 3.18: Extracted Ucode8 Chips*

The extracted Ucode8 chip is stuck into the RFID antenna with the help of copper tape. Copper tape attaches an antenna chip to an RFID tag because it provides a reliable electrical connection between the chip and the antenna. By using copper tape, the antenna chip can be securely attached to the antenna, ensuring that the electrical relationship between the two components is solid and stable. This helps to ensure that the RFID tag can accurately transmit and receive signals, which is critical for the system's successful operation. The completed RFID can be seen in Figure 3.19.

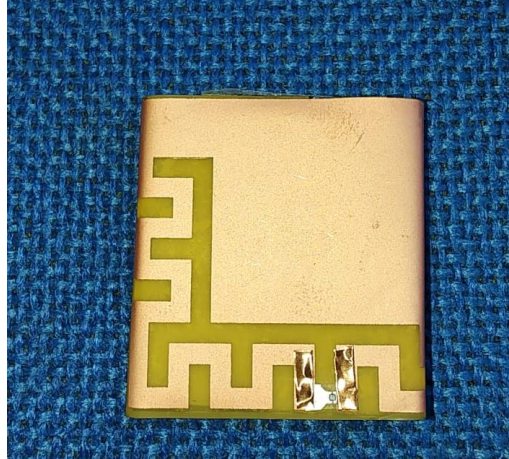


*Figure 3.19: Completed RFID Tag*

### **3.2.9 Measurement**

The Tagfomance System is used to measure the RFID antenna performance. The RFID is placed inside the anechoic chamber for measurement. An anechoic section is a specialized room designed to absorb sound and electromagnetic waves, providing a near-perfect environment for measuring radio frequency signals such as those used in RFID systems. There are several reasons why RFID is measured in an anechoic chamber, including reducing interference as the anechoic chamber is designed to minimize interference from external sources, such as other radio signals, which can affect the accuracy of RFID measurements. This helps ensure that the RFID system is accurately measuring the performance of the tag and reader. Besides, it allows reproducing-controlled conditions. An anechoic chamber allows for the reproduction of controlled test conditions, enabling consistent and repeatable measurements of RFID performance. This is important for accurate and reliable testing and comparison of different tags and readers. Finally, an anechoic chamber eliminates reflections from walls and other surfaces, impacting the accuracy of RFID measurements. Hence ensure that the RFID system is accurately measuring the performance of the tag and reader without interference from reflections.

The read pattern measurements are crucial for designing passive UHF RFID tags because they demonstrate how the reader antenna's response to the tag's activation will affect the radiation pattern. Most metal-mountable RFID tag designs have the greatest radiation intensity at the bore-sight angle ( $\theta = 0^\circ$ ). This proposed tag's emission

pattern responds to the reader antenna in a quasi-isotropic manner, which is advantageous for tracking applications. The read distance patterns are measured at a frequency resonating at the usable UHF spectrum in three separate planes: the x-y, x-z, and y-z planes. The 3 distinct cut planes radiation characteristics can be used to estimate the 3D radiated detection distance pattern by the tag-under-test. The radiation pattern for read distance in Figure 3.20 (Moh et al., 2018) is generated from both the x-z and y-z planes, following the spherical coordinate system pattern. If the UHF RFID tag is rotated about the z-axis to obtain the read distance pattern in the x-y plane, the polarization of the EM wave in the bore-sight direction will be specific to the UHF RFID tag being tested. This will result in the display of the read distance pattern in the x-y plane.

The measurement of the read range and performance of the RFID tags is done by using the Tagformance system. Firstly, the Tagformance system needs initial calibration by stick the calibration chips onto the dielectric foam and put inside the Tagformance machine, as seen in Figure 3.21. After the calibration, the completed RFID tag is stick embedded into the metal with a metal plate area of  $(200 \times 200 \text{ mm}^2)$  with an embedded metal frame size of  $(140 \times 140 \times 10 \text{ mm}^3)$  as seen in figure 3.22. Besides, the x-z plane and y-z plane measurements can be refer in Figures 3.23 and 3.24, respectively. The data is then collected using the build Tagformance UHF Software.

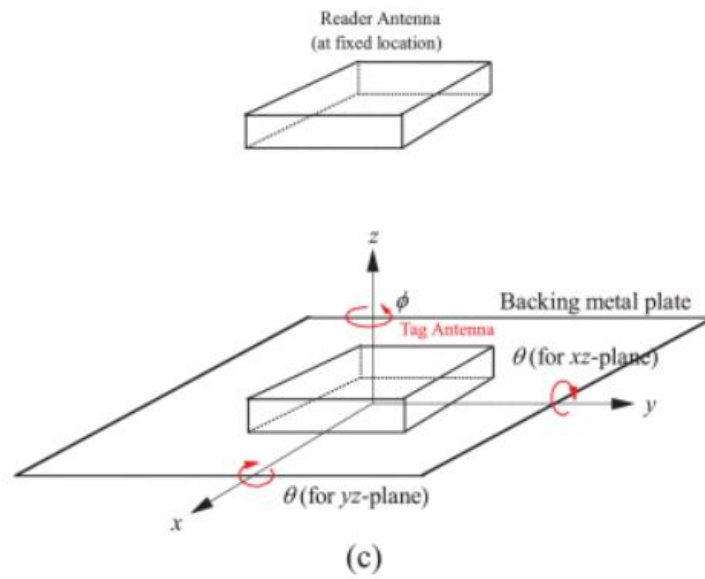


*Figure 3.20: The measurement setup to obtain the read distance pattern across all the three different planes.*

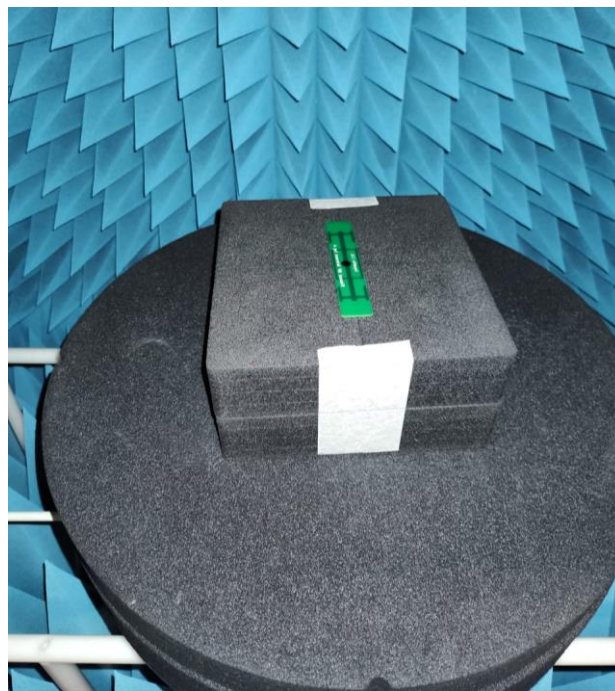


*Figure 3.21: Calibration of the Tagformance system*

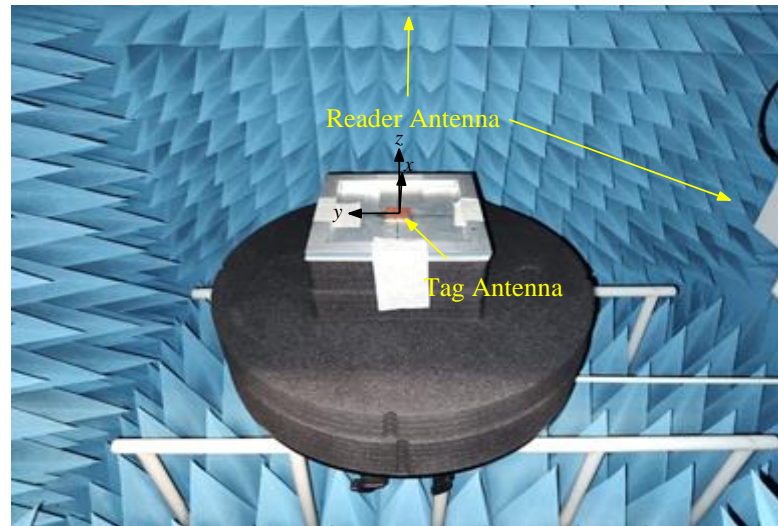


*Figure 3.22: x-y plane measurement in anechoic chamber*

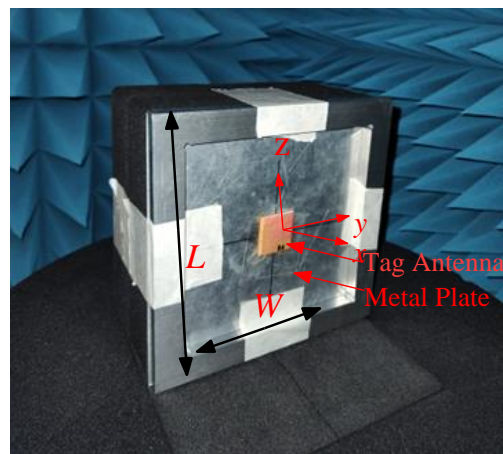


*Figure 3.23: x-z plane measurement in anechoic chamber*

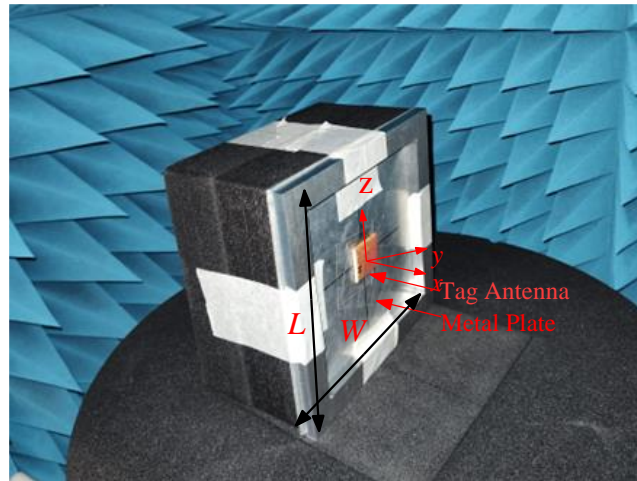


*Figure 3.24: y-z plane measurement in anechoic chamber*

### 3.3 Summary

In summary, the methods for designing the miniature RFID used in embedded tracking systems include researching and reviewing journal articles on similar topics, designing the antenna using CST simulation, manufacturing the physical prototype, and validating the design using Tagformance to determine physical antenna performance.

During the research project, some obstacles were faced. One of the obstacles is that the CST simulation's simulated result needed to be more accurate due to a bug in the applications as the designed antenna was changed and modified continuously. The result obtained from the antenna, including the S-parameter and far-field gain, was not accurate as the simulation was done by referring to the cache file of the previous unmodified antenna. Hence, causing the simulated result to be inaccurate. The solution is to copy and create a new file to prevent this issue. By doing this, the CST simulation will restimulate the antenna rather than continue the simulation using the cache file of the previous result.

## CHAPTER 4

### RESULTS AND DISCUSSION

#### 4.1 Introduction

The design starts with the antenna design simulation in CST simulation 2021. The simulated results of the S-parameter, Z-parameter, and far-field gain, resonant frequency, input impedance, currents distribution, realized gain, and radiation pattern are studied and discussed, were analysed. The parameter sweep was used to optimize the antenna further to obtain the best performance of the antenna to fulfil the application objectives. The antenna prototype is fabricated using chemical etching methods, with the performance measured and recorded using a Tagformance system.

The simulated proposed tag antenna is simulated on a metal plate with a size of  $(200 \times 200 \text{ mm}^2)$  and embedded inside a metal frame of  $(140 \times 140 \times 20 \text{ mm}^3)$ . The realized gain, resonant frequency, read range, and impedance matching are recorded. Multiple parametric analyses are done, including different meandered strip widths, metal cavity size, and metal cavity depth are studied to determine the effect of varying variations on the performance of the antenna. On the other hand, the fabricated antenna is measured on the Tagformance system to determine the read range and polarization in x-y, x-z, and y-z planes.

The proposed tag antenna diagram can be referred to in Figure 4.1, with dimensions of the antenna given as  $w_a$  and  $l_a$  is the width and length of the antenna size, which is given as 30 mm. The  $h$  is height of the dielectric substance foam with a dimension of 3.2 mm.  $w_3$  is the width of the meandered strip, and  $l_3$  is the height of the meandered strip, which both have a dimension of 2 mm. The  $w_1$  and  $l_1$  are the size of the main radiating patch, has dimension of 22 mm and 26 mm, respectively.  $l_4$  is the length of the shorting path with a dimension of 2 mm, and  $l_2$  is 6 mm.

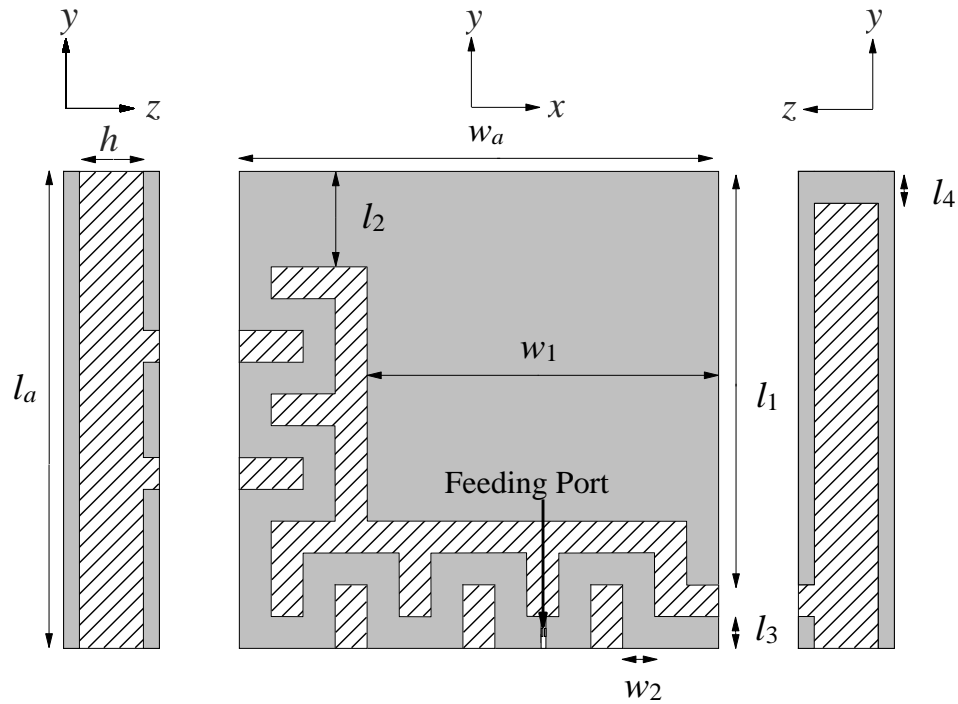
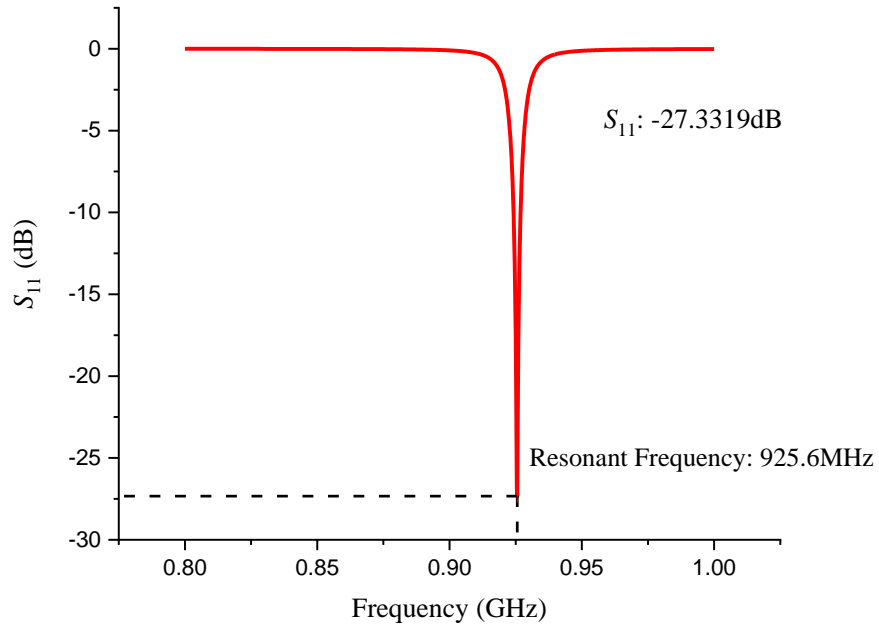


Figure 4.1: Top and side views of the proposed antenna

#### 4.2.1 Result

The S-parameter ( $S_{11}$ ) of the proposed antenna, when the RFID tags are stuck on top of the metal plate with a size of  $(200 \times 200 \text{ mm}^2)$ , is shown in Figure 4.1. The result obtained has the S-parameter has a  $-27.3319\text{dB}$  of impedance matching between the source and the antenna at the resonant frequency of  $925.6 \text{ MHz}$ . This is because the proposed antenna, together with the metal plate, has a total impedance of  $13.7812 \Omega + 188.7862 j\Omega$ , as referring in Figure 4.3, as the antenna chip used is the Code 8 microchip. When refereeing to the datasheet of the Ucode8, the chip had an impedance

of  $13 \Omega - 190 j\Omega$ . Therefore, the inductance in the antenna cancels the capacitance of the Ucode8 chips. Hence, the antenna has an impedance match of 99.8%.



*Figure 4.2: The simulated  $S_{11}$  (Impedance matching) when RFID tags on the metal plate*

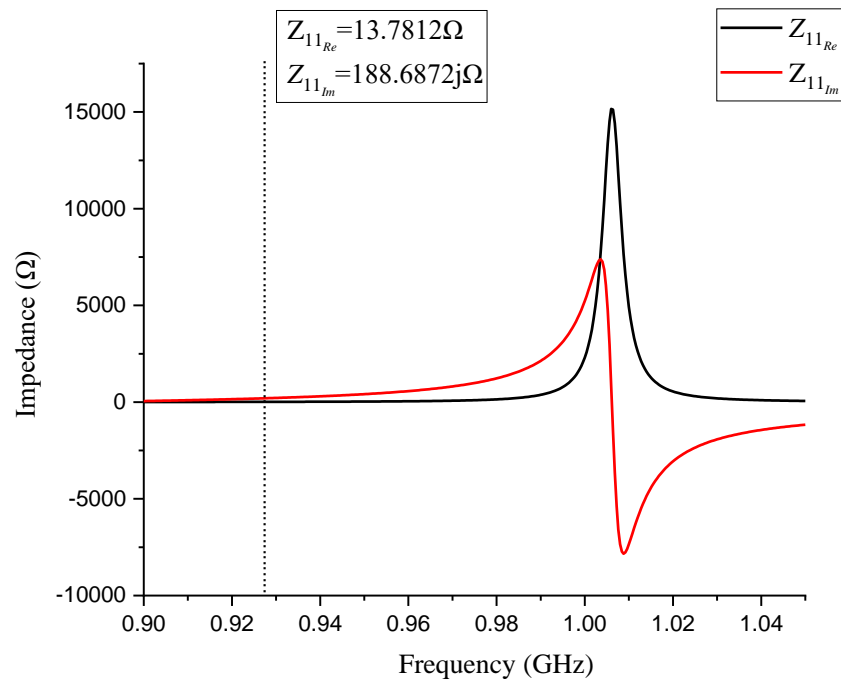


Figure 4.3: Z parameter of the RFID tags on metal plate.

On the other hand, The S-parameter ( $S_{11}$ ) of the proposed antenna when the RFID tags are embedded in the metal plate with a size of  $(200 \times 200 \text{ mm}^2)$  and the metal frame of  $(140 \times 140 \times 20 \text{ mm}^3)$  is shown in Figure 4.4. The result obtained was that the S-parameter has a -34.9354 dB of impedance matching between the source and the antenna at the resonant frequency of 926 MHz. Hence, the antenna has an impedance match of 99.99%. This is because the proposed tag antenna has a Z-parameter of  $13.858 + 191.372 j \Omega$ , as seen in figure 4.5 at the resonant frequency is almost solely resistive at 926 MHz, where the antenna's and Ucode8's capacitance and inductance cancel each other out. The proposed antenna can therefore operate effectively in the 860–960 MHz UHF range.

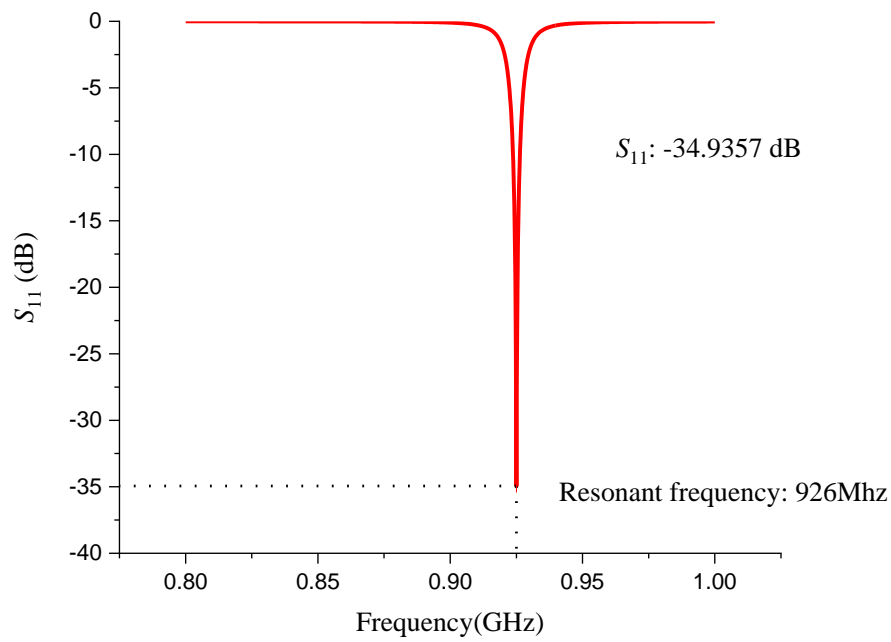


Figure 4.4: The simulated  $S_{11}$  (Impedance matching) when RFID tags embedded in metal plate.

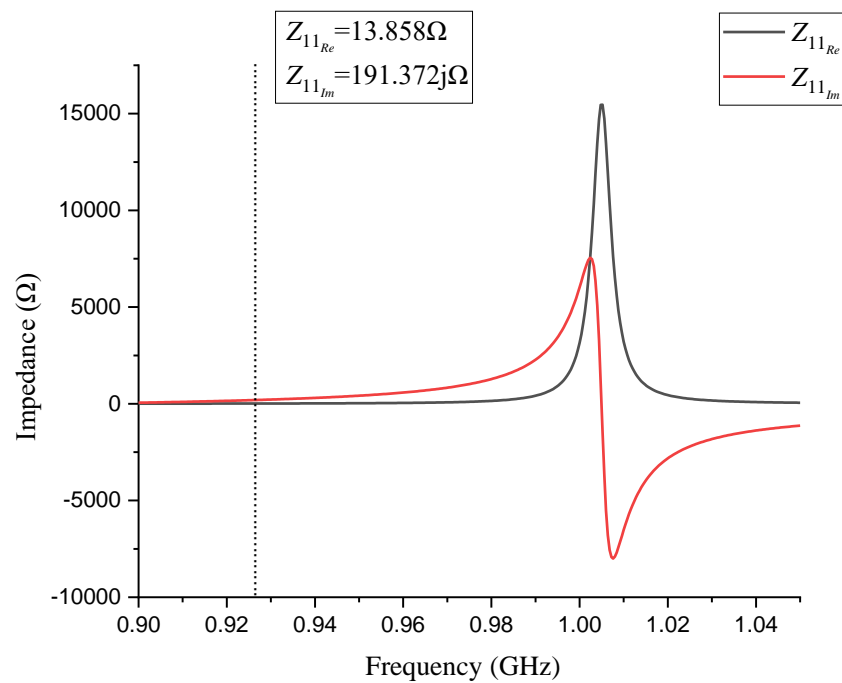


Figure 4.5:  $Z$  parameter of the RFID tags embedded in metal plate.

#### 4.2.2 Meandered Line Width Parametric analysis

Parametric analysis is an essential process in designing and implementing RFID systems. The parametric analysis involves examining the various parameters that affect the performance of an RFID system, such as the size and length of the RFID patch antenna and the depth of the embedded metal plate. By analysing these parameters, the performance of an RFID system for a particular application and environment can optimize. Some of the benefits of parametric analysis in doing RFID include improved accuracy by optimizing the parameters of an RFID system. It can improve the accuracy of data capture and reduce errors in the data processing. Besides, the optimization can increase the read range of the RFID By adjusting the power level and frequency of the RFID reader, allowing for more efficient and effective data capture.

Lastly, by optimizing the performance of an RFID system, The size and thickness of the antenna can be optimized to reduce the raw material and labor cost needed for the fabrication of the antenna.

The width of the meandered strip  $w_2$  is optimized by doing a parametric analysis from  $w_2 = 1.6$  mm to  $w_2 = 2.4$  mm with an increment of 0.2mm is done. The  $S_{11}$ , which is the impedance matching of the antenna, is plotted as shown in Figure 4.6. From the figure, with the increase in the width of the meandered strip, the resonant frequency shifted from 0.96 GHz to 0.895 GHz. On the other hand, the impedance matching increases when the width of the meandered strip increases from -23dB to the highest of -34.5 dB when  $w_2 = 2.2$  mm. However, when the  $w_2$  increases to 2.4mm, the impedance matching between the Ucode8 chips with the antenna patch reduces to 32.3 dB. From the parameter analysis, we can determine that when  $w_2 = 2.2$  mm, it has the highest impedance matching efficiency of 99.99% of -32.3 dB compared to the second highest of only -27.3 dB, which has an efficiency of 99.8%. However, even though  $w_2 = 2.2$  mm has the highest efficiency, the resonant frequency falls on 910 MHz compared to 926 MHz. Even though both fall inside the US UHF RFID bandwidth (902-928 MHz), higher frequencies result in a better read range in RFID. Higher-frequency radio waves have a shorter wavelength and are more directional, meaning they can travel longer distances without getting scattered or absorbed by obstacles. Additionally, the  $w_2 = 2$  mm is easier to be fabricated, and the slimmer

meandered strips result in lesser copper used, causing reduce in fabrication cost and making it more environmentally friendly by using lesser earth's precious metal.

This is because when the width of the meandered line is too thin, it reduces the overall conductive path of the copper line. Following ohms law, the wire resistance is inversely proportional to the wire's effective area. On the other hand, as the meandered line in the proposed antenna is shaped like a snake-like structure, if the width of the line is too large, the gap between wires will decrease. Hence the two conductive paths will cause the unwanted d coupling effect and cause the antenna patch to increase the inductive reactance of the system and causes energy loss as the current is diverted from the intended path and absorbed by the adjacent conductor.

The Z-parameter matrix is a  $2 \times 2$  matrix, and each matrix element is a complex impedance. The fundamental part of the impedance represents the resistive component, while the imaginary part represents the reactive component. Form Figure 4.7, when the meandered line increases from  $w_2 = 1.6$  mm to  $w_2 = 2.4$  mm, the peak real impedance increases from the 12000  $\Omega$  to 18000  $\Omega$ , and imaginary reactance reduces from -6180  $\Omega$  to -9383  $\Omega$ .

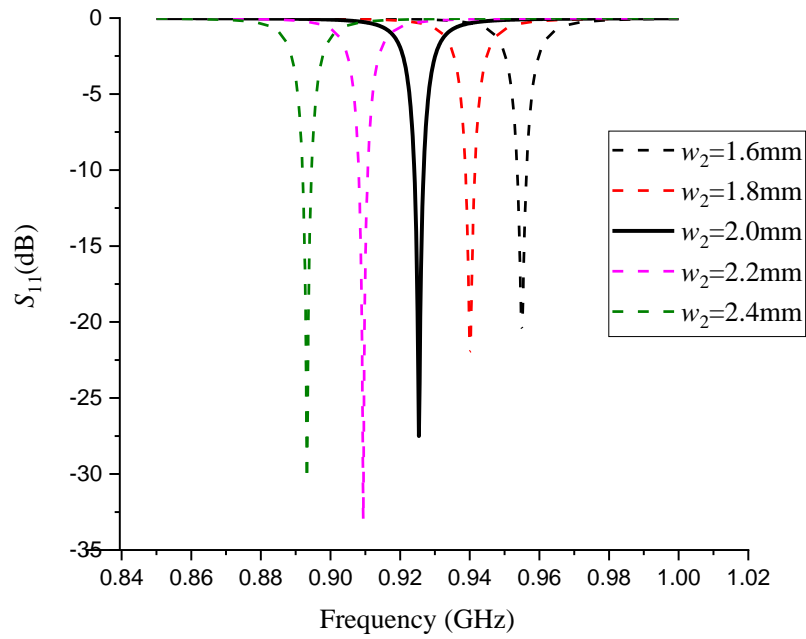


Figure 4.6: Parametric analysis of the  $S$ -parameter on the width of the meandered strip

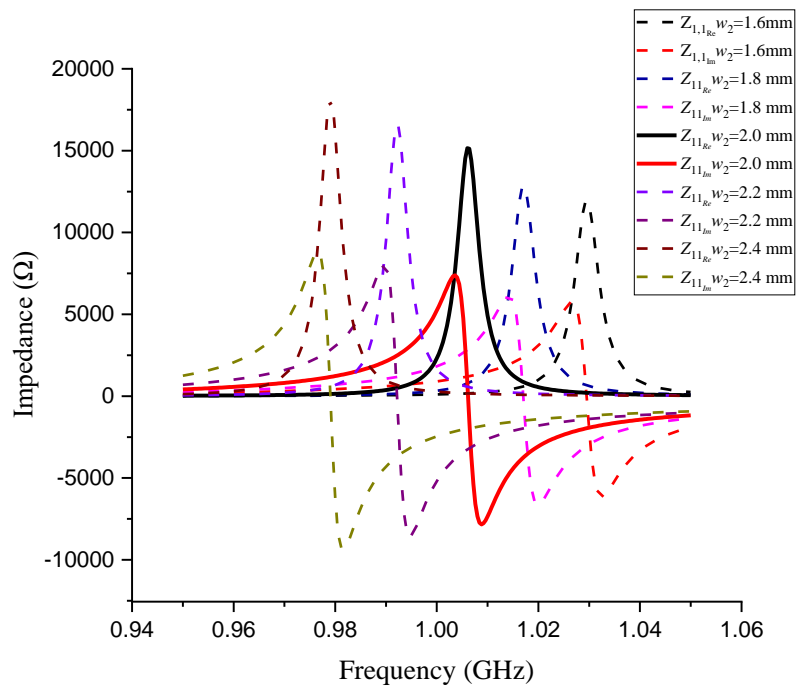


Figure 4.7: Parametric analysis of the  $Z$ -parameter on the width of the meandered strip

### 4.2.3 Metal Cavity Depth Parametric Analysis

Other sets of parametric analysis are performed by altering the depth of the embedded metal cavity from 0m (On the surface) to 19 mm. Figure 4.8 shows the simulation of the linear realized gain when the depth of the cavity,  $d=19$  mm, is shown below. From figure 4.9 and 4.10, when the depth of the cavity increases from 0 mm to 19 mm, the realized gain and the read range shows similar properties and trend. The read range and the realized gain increase when the cavity increases from 0 mm to 10 mm. At the simulation's resonant frequency, 926 MHz, the read range increases from 18.77 m to 18.88 m, and the realized gain increase from 0.376 dB to 0.425 dB. On the other hand, when the depth of the cavity increases from 10mm to 19mm, the read range and realized gain decreases slightly from 18.88 m to 18.23 m, whereas the realized gain increases from 0.425 dB to 0.118 dB.

This is because the radio wave transmission follows Faraday Law. According to Geroge et al. (1984), Faraday Law explained that when an electrically conductive material, metal in this experiment, is placed in a changing magnetic field, it can induce an electric current to flow within the material. When the RFID tag is placed deeper inside the metal, the metal acts as a shield that blocks the magnetic field from reaching the tag and reduces the wave to be transmitted. This causes the tag to experience a weaker magnetic field than outside the metal. As a result, the induced electric current within the tag is weaker, which reduces the signal strength and the tag's read range. Besides, the metal can cause a phenomenon is known as eddy currents, which are circular electrical currents that flow within the metal. These eddy currents can absorb energy from the magnetic field, further reducing the strength of the field and making it more difficult for the tag to communicate with the reader.

However, when the deep of the metal increase from 0 mm to 10 mm, the read range increase slightly. This is because of the detuning phenomena where metal near the RFID tag can alter the antenna's resonant frequency, causing it to shift the resonant frequency and the impedance matching between the tags and the Ucode8 chips. As the depth is 10 m, the impedance matching is -35 dB which is around 100% match which causes the increment in the read range.

Besides, when  $d=5$  mm, when the frequency starts from 900 MHz, the read range is only 1.86 m and increases to 18.7 m at the resonant frequency. However, when the frequency exceeded beyond resonant frequency, the read range reduced and only had 1.17 MHz at 1000 MHz.

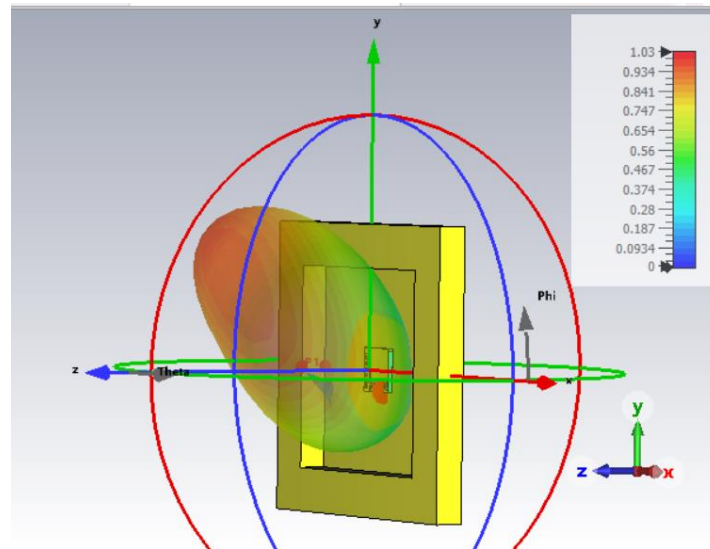


Figure 4.8: Linear realized gain when Depth = 19mm

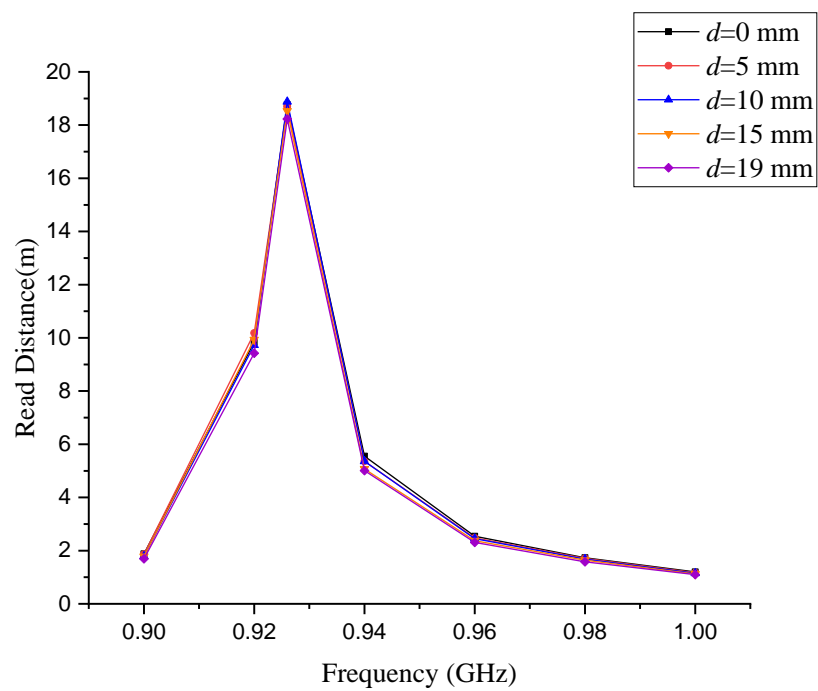


Figure 4.9: Parametric analysis of the Read Range with increasing embedded metal depth,  $d$

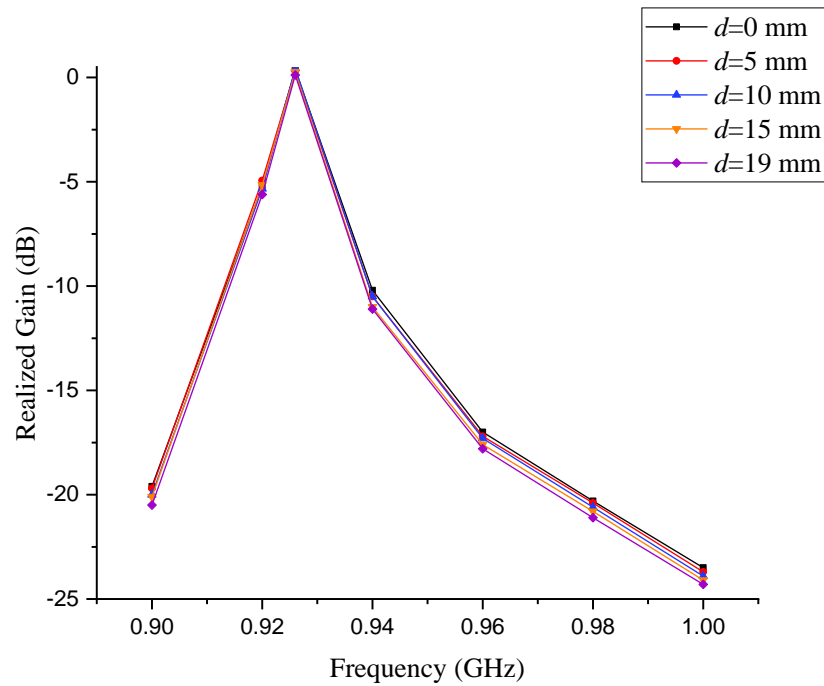


Figure 4.10: Parametric analysis of the Realized Gain (dBm) with increasing embedded metal depth,  $d$

#### 4.2.4 Metal Cavity Size Parametric Analysis

Other sets of parametric analysis are performed by altering the size of the metal cavity for the embedded RFID from 50mm to 170mm, which can be referred to in Figures 4.11 and 4.12, respectively. From figure 4.13 and 4.14, when the width of the cavity increases from 50mm to 170mm, the realized gain and the read range shows similar properties and trend, where the gain and the read range increases with the increment of the cavity size. At the simulation's resonant frequency, 926 MHz, the read range increases from 15.90 m to 18.78 m, and the realized gain increase from -1.07 dB to 0.337 dB with the increment of the cavity size. This is because when the metal cavity is smaller, the electromagnetic generated by the RFID antenna has more hindrance to escape to the atmosphere by following Faraday's law. The metal cavity is an electrically conductive material. Hence, the metal cavity can absorb the electromagnetic wave generated. Therefore, reducing the realized gain and read range

From the simulation, it can be proved that the proposed antenna can be used in the embedded metal cavity as even though the metal cavity is tiny, the RFID can

generate a high read range with a good realized gain of 15.9 m. This is because the proposed RFID antenna generated a directional wave and caused the metal cavity to have little effect on the performance of the RFID tags.

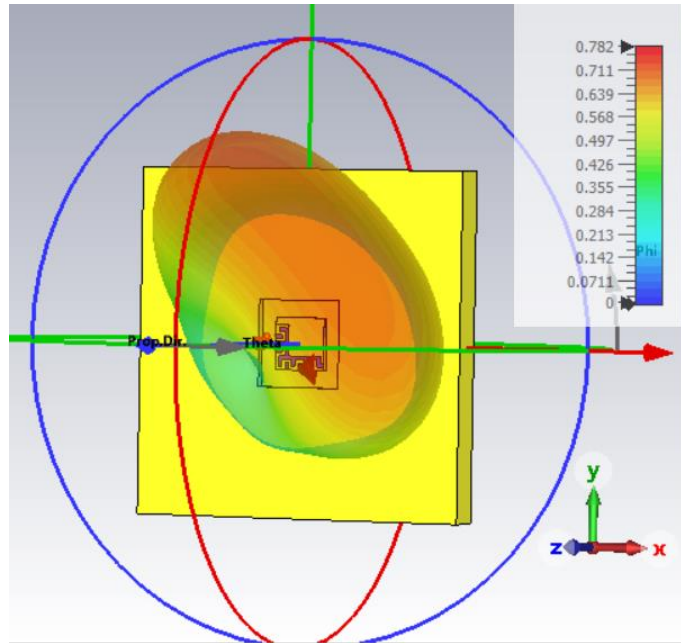


Figure 4.11: Linear realized gain when cavity size,  $w = 50\text{mm}$

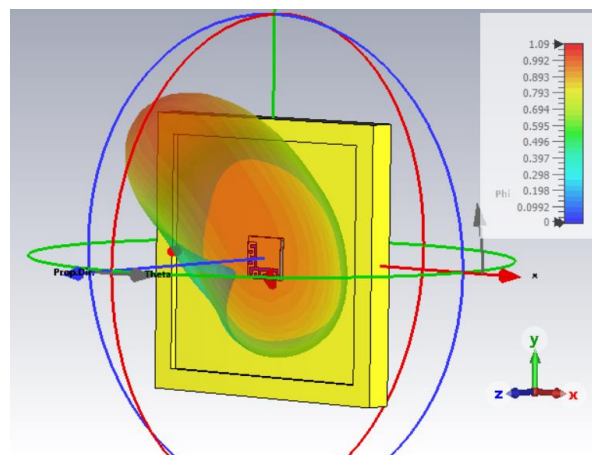


Figure 4.12: Linear realized gain when cavity size,  $w = 170\text{mm}$

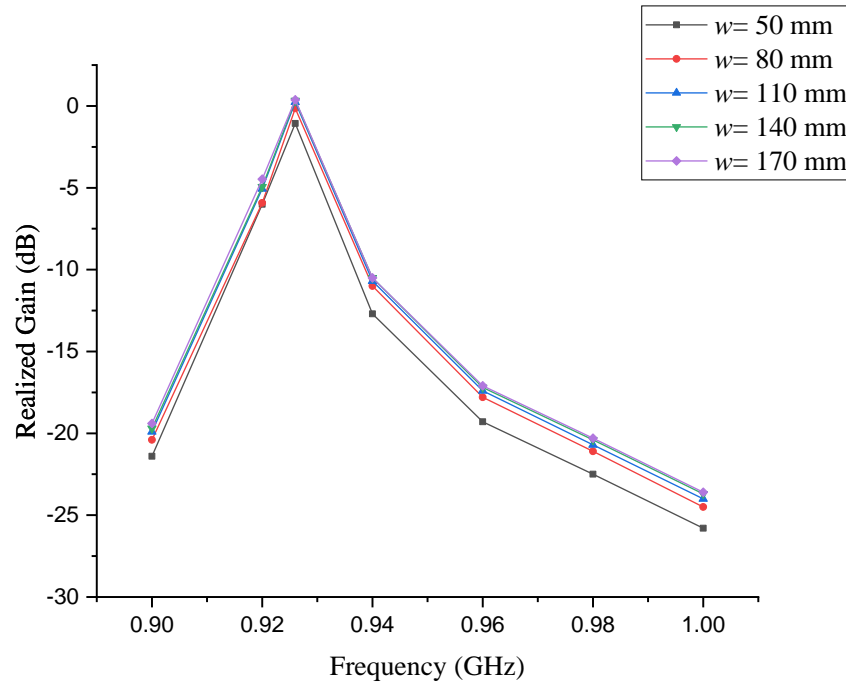


Figure 4.13: Parametric analysis of the Realized Gain (dBm) with increasing embedded metal cavity size,  $w$

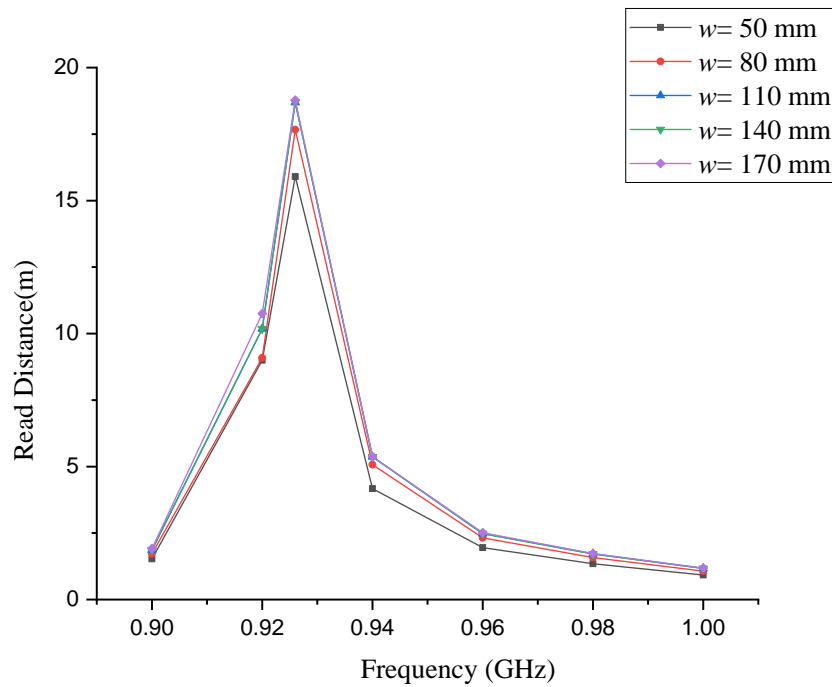


Figure 4.14: Parametric analysis of the read range with increasing embedded metal cavity size,  $w$

### 4.3 Prototype Measurement

The physical prototype is measured on the metal surface and embedded in the metal cavity 5 mm deep. Three different orientations of the read range are obtained. Figure 4.15 shows that x-y Plane's read range is the highest at the resonant frequency at 926 MHz for both experiments. However, the Read range is higher on metal, which is 5.5 m, whereas the embedded RFID has a slightly lower read range forward of 5.4 m.

From the polar diagram in Figure 4.16, from 0 degrees to 210 degrees, both metal and metal experiments generate similar read ranges at 926MHz, however beyond 210 to 360Degrees, the read range in the on-surface RFID antenna produces a better-read range with a peak range of 7.9m at 315 degrees compared to only 7m with the embedded RFID antenna. A near null-point lobe located at  $\theta = 45^\circ$  ( $\varphi = 180^\circ$  cut) is observed with a read range of 0m and its exact opposite direction and  $\theta = 225^\circ$ , whereas the main lobe direction is located at  $\theta = 135^\circ$  ( $\varphi = 180^\circ$  cut) and  $\theta = 315^\circ$  ( $\varphi = 0^\circ$  cut) with the read range with peak range of 7.9 m and 7 m for embedded and on surface respectively.

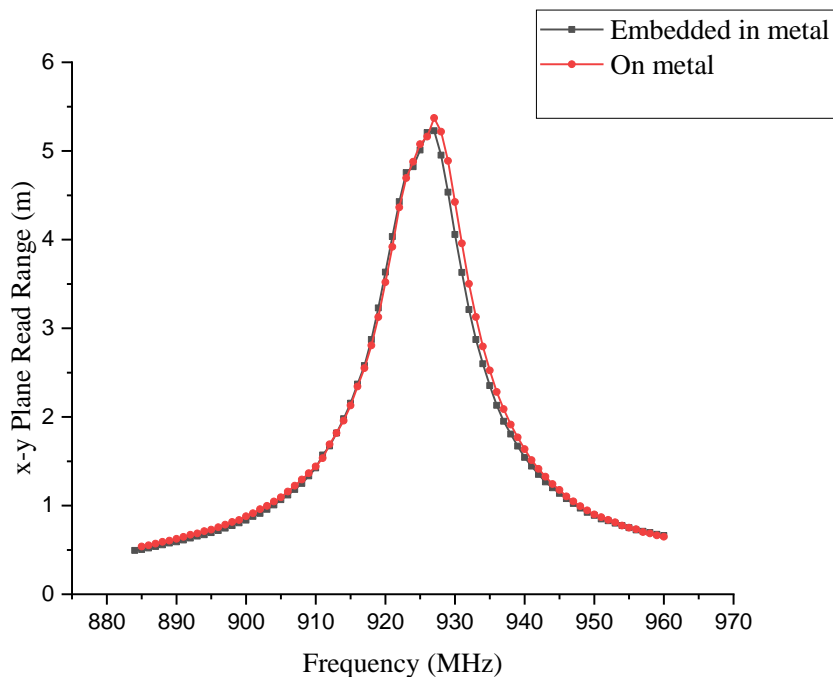
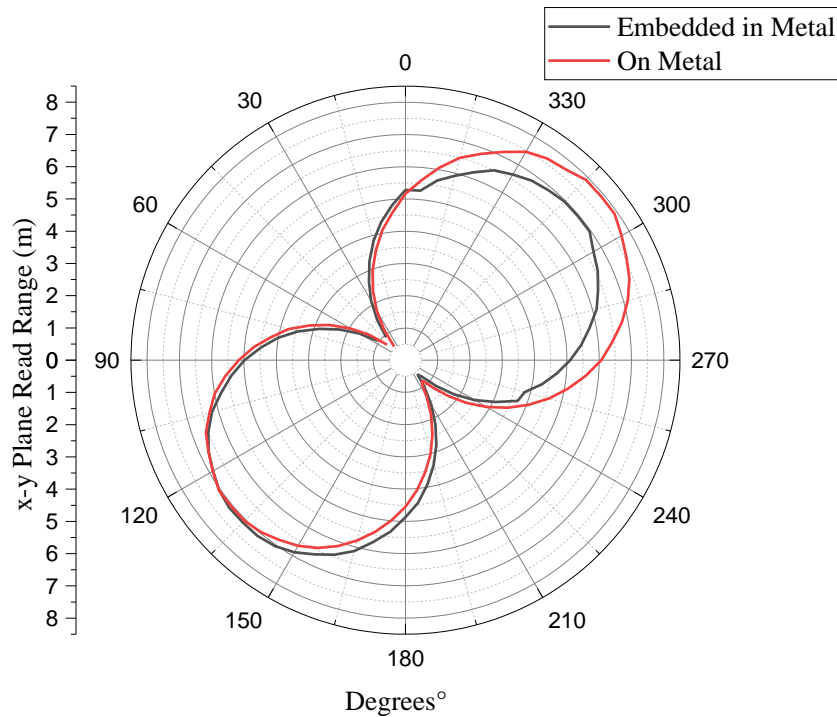


Figure 4.15: x-y plane Read Range of RFID Prototype between In metal and On metal measurement

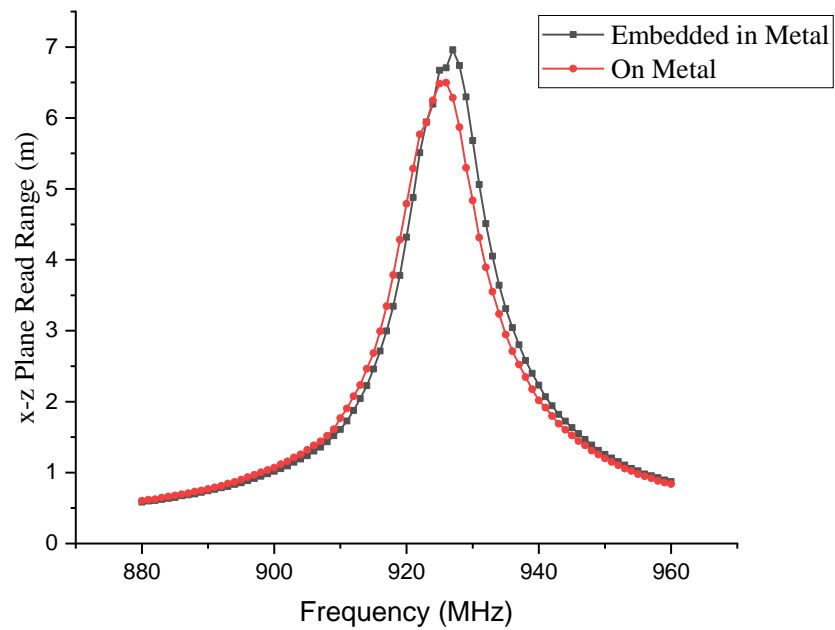


*Figure 4.16: x-y plane Polar Read Range of RFID Prototype between In metal and On metal measurement*

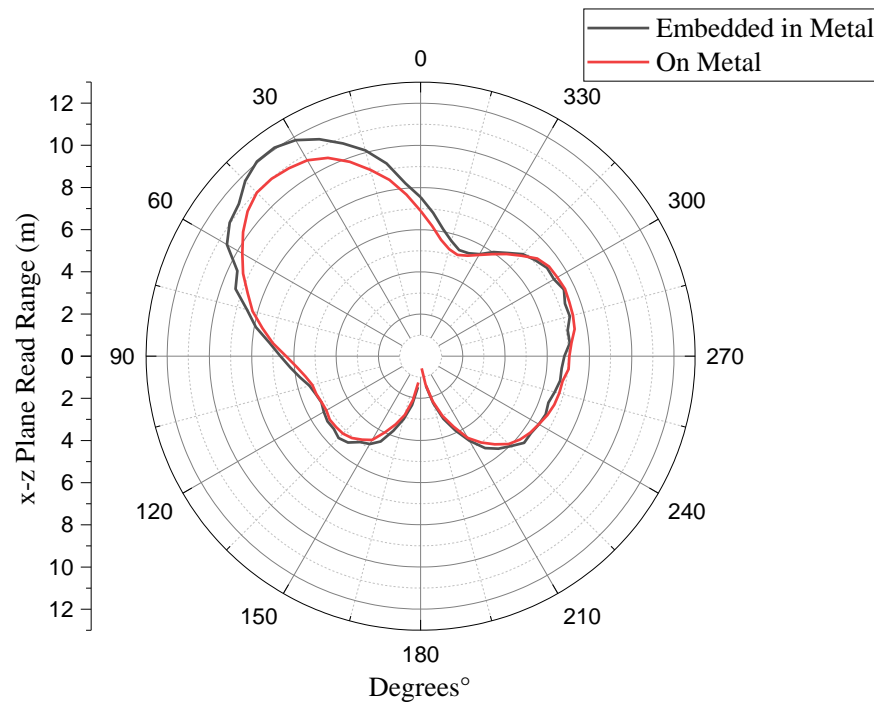
The Read range and polarization for the x-z plane are further studied to study the RFID antenna's true read range. According to Figure 4.17, 2 experiments are done where one RFID antenna is embedded into the metal cavity and the other is attached to the antenna's surface. The experiment shows a similar result and pattern where the read range increases from 880 MHz to the peak at the resonant frequency at 926 MHz and reduces at 960 MHz. The embedded-in-cavity experiment has a higher peak read range at 6.96 m compared to only 6.26 m when the RFID tags are attached to the metal surface. Besides, the resonant frequency shifts slightly to a higher frequency at 927 MHz compared to 926 Mhz.

Figure 4.18 shows the measured physical prototype's x-z plane polar read range when embedded in metal and on metal. From the figure, both experiments show similar readings and patterns where the antenna generates the highest read range at  $37^\circ$  in the z direction. This is due to the RFID antenna design having the main radiating patch at one of the corners and not at the centre of the antenna. Hence causing, the maximum radiating far field is slanted at  $\theta = 40^\circ$ . Besides, the polar graph shows that

the antenna generates 0 far-field with 0 read range forward when the angle is 180 degrees. This is due to the antenna stick at the back of the metal where the antenna's ground is connected. Hence, following Faraday's Law, the electrical field cannot escape electrical conducting material, causing no generated radiating field. From both measurements, the RFID tags' read range is higher when the tags are embedded in the metal cavity, with a peak read range of 12.05 m compared to only 10.96 m when the tags are on the metal surface.



*Figure 4.17: x-z plane Read Range of RFID Prototype between In metal and On metal measurement*

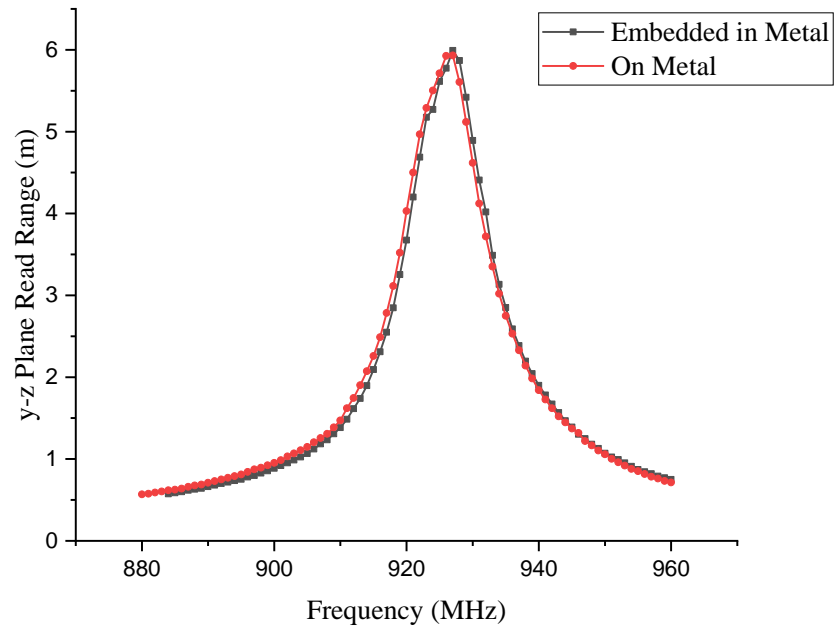


*Figure 4.18: x-z plane Polar Read Range of RFID Prototype between In metal and On metal measurement*

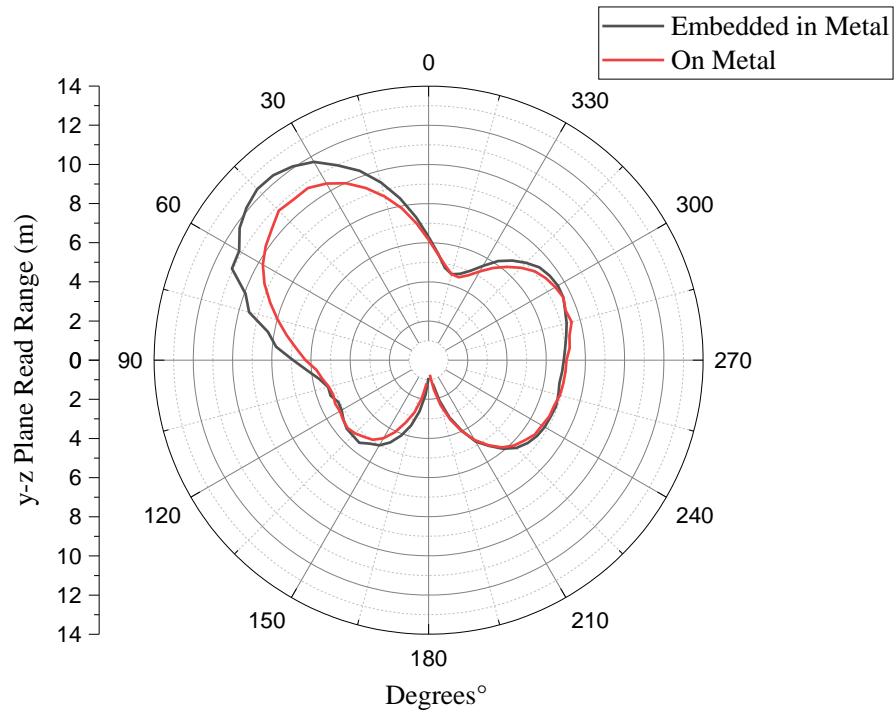
The Read range and polarization for the y-z plane are further studied to study the RFID antenna's true read range. According to Figure 4.19, 2 experiments are done where one RFID antenna is embedded into the metal cavity and the other is attached to the antenna's surface. The experiment shows a similar result and pattern where the read range increases from 880 MHz to the peak at the resonant frequency at 926 MHz and reduces at 960 MHz. The embedded-in-cavity experiment has a higher peak read range at 5.99 m compared to only 5.9 3m when the RFID tags are attached to the metal surface. Besides, the antenna has the same resonant frequency of 926 Mhz when the antenna is tagged on the surface and embedded inside the metal cavity.

Figure 4.20 shows the measured physical prototype's x-z plane polar read range when embedded in metal and on metal. From the figure, both experiments show similar readings and patterns where the antenna generates the highest read range at  $40^\circ$  in the z direction. This is due to the RFID antenna design having the main radiating patch at one of the corners and not at the centre of the antenna. Hence causing, the maximum radiating far field is slanted at  $\theta = 40^\circ$ . Besides, the polar graph shows that

the antenna generates 0 far-field with 0 read range forward when the angle is 180 degrees. From both measurements, the RFID tags' read range is higher when the tags are embedded in the metal cavity, with a peak read range of 12.32 m compared to only 10.70 m when the tags are on the metal surface.



*Figure 4.19: y-z plane Read Range of RFID Prototype between In metal and On metal measurement*



*Figure 4.20: y-z plane Polar Read Range of RFID Prototype between In metal and On metal measurement*

#### 4.4 Result Summary

The simulated read range forward for the embedded antenna at the resonant frequency of 926MHz is 18.7m. On the other hand, the peak read content forward for the physical prototype in the embedded metal cavity is only 12.32m. The first reason is that the peak radiating angle of the antenna is at  $\theta = 37^\circ$ . However, the physical measurement is done in sensitivity of  $\theta = 5^\circ$ . The peak radiating angle cannot be determined hence the lower read range. Secondly, the peak read range is at  $\theta = 37^\circ$  in x and y directions. Unfortunately, the measurement only can obtain from  $37^\circ$  in x direction and  $\theta = 37^\circ$  in the y direction separately. For example, during the x-z plane measurement, the measurement obtains only  $37^\circ$  in x direction, which cannot determine the peak in the Y direction. Hence cannot obtain the peak output at  $\theta = 37^\circ$  x and  $\theta = 37^\circ$  y coordinates.

Thirdly, the prototype measurement is lower due to human error in fabricating the RFID tag antenna. The etching and fabrication process to folding and sticking of

the antenna has multiple risks of human error in reducing the optimum environment for the antenna to perform.

One of the human errors is the manufacturing tolerances. During the fabrication, the copper etching process may be imperfect and cause the edges to be irregular and not perfectly straight, as the uneven edges can have a current-losing effect and cause the loss of electrical and magnetic waves. Besides, the simulated antenna may have been designed with idealized material properties, which may not reflect the real-world properties of the materials used in the physical prototype. Real-world materials may have imperfections, such as variations in thickness, impurities, or defects, which can affect the antenna's performance. For example, the copper sheet material is highly reactive and will become rusted when exposed to open air for an extended period, as the copper can react with oxygen and produce copper oxide. Hence the oxidation process can reduce the performance of the tag antenna. Next, while the antenna is folded with the Styrofoam, the soft characteristic of the Styrofoam may cause the whole RFID antenna to deform, causing the high of the antenna,  $h$  to change and change the properties of the RFID antenna.

One of the essential factors of the lower read range in the prototype is that the Ucode8 chips are extracted from the existing RFID tags and manually stuck into the proposed RFID antenna rather than perfectly embedded into the copper strips in the RFID antenna fabrication. Therefore, causing poor coupling between the antenna and the RFID chip. When the antenna chips are embedded into the RFID tag, they are placed close to the RFID chip, which helps ensure good coupling between the two components. When the chips are stuck onto the RFID tag, there may be a more significant separation between the chips and the RFID chip, leading to weaker coupling and reduced read range. Furthermore, it causes alignment issues as the Ucode8 is stuck onto the RFID tag. Achieving optimal alignment may be more challenging, leading to reduced read range. Next, the sticking of Ucode8 chips causes interference as the antenna chips are stuck onto the RFID tag. There may be interference between the chips and the RFID chip, which can degrade performance. Various factors, including reflections, scattering, and electromagnetic interference can cause this interference.

*Table 4.1: The comparison of UHF RFID with miniature metal mountable properties.*

Proposed Tag	Dimension	Metal mountable / Metal Embedded	Double layer	Maximum Read Distance
Lee et al (2020)	$25 \times 18.75 \times 3.1 \text{ mm}^3$	Metal Mountable	Yes	14.6 m
Bansal et al. (2019)	$68 \times 34 \times 0.8 \text{ mm}^3$	No	No	14.5 m
Ng et al. (2019)	$25 \times 25 \times 3.2 \text{ mm}^3$	Metal Mountable	Yes	11.9 m (7m on metal)
Lee, et al., (2019)	$40 \times 40 \times 3.1 \text{ mm}^3$	Metal Mountable	Yes	9.2 m
Proposed Tag antenna	$30 \times 30 \times 3.1 \text{ mm}^3$	Metal Mountable and Metal embedded	No	18.88 m (12.3 m Measured)

According to Table 4.1, in the first design from Lee et al. (2020), the antenna has a good read range of 14.6 m with a miniature size of only  $25 \times 18.75 \times 3.1 \text{ mm}^3$ . However, the antenna has a complex structure with folded double-layer design to have an extra coupling stud that can increase the antenna's realized gain and read range. Even with the complex system, the antenna's read range is only 14.6 m which means the proposed antenna's simulated read range is further than the antenna, and with a more proper fabrication and measurement system, the proposed antenna can have a different measurement read range. Similarly, the design from Ng et al. (2019) has the same properties of a miniature size of  $25 \times 25 \times 3.2 \text{ mm}^3$  with folded double-layer structure with a metal mountable application. However, the read range is only 11.9 m with 7M on the metal application, which is far lower than the proposed antenna.

On the other hand, the design from Lee et al. (2019) and Bansal et al. (2019) has a large antenna structure of  $40 \times 40 \times 3.1 \text{ mm}^3$  and  $68 \times 34 \times 0.8 \text{ mm}^3$ , respectively. Even with the large size, the antenna only has a read range of 9.2 m and 14.5m. Moreover, the design from Bansal et al. (2019) cannot be mountable on metal. By

comparing the proposed antenna with the reviewed literature antenna, the proposed antenna has the most extended maximum range in simulation, which is 18.88 m, despite the measured, fabricated prototype read range being 12.3 m. However, the other literature antenna has more complex antenna structures, such as folded double layer in Ng et al. (2019), Lee et al., 2019 and Lee et al. (2020), and some of the antenna structures have bigger structure sizes, for example in Bansal et al. (2019) and Lee et al., 2019.

Hence, the proposed antenna has the most extended simulated maximum read range of 18.88m and a decent 12.3 m of measured read range with metal mountable and embedded metal application with a simple single-layer structure and miniature size. The proposed antenna has the furthest read range in single layer antenna from the literature review and the longest read range compared to a similar miniature size antenna.

## CHAPTER 5

### CONCLUSION AND RECOMMENDATIONS

#### 5.1 Conclusion.

In conclusion, the objectives established earlier have been successfully achieved by completing this final year project thesis. During the project, the meandered line structure antenna analysis revealed its usefulness for antenna design, specifically for passive UHF RFID tag applications. It was discovered that this type of antenna could provide a highly realized directional radiation pattern with high gain, making it suitable for metal-mountable and embedded metal applications. Multiple impedance matching and resonant frequency tuning techniques, such as the meandered line and shorting stub techniques, have been explored.

Additionally, various miniaturization techniques for the proposed tags have been well-equipped by other literature, including using a high dielectric constant and shortening the path between the radiating patch and the ground plane. These techniques enhance the inductance of the antenna structure, which helps to tune down the resonant frequency. It is important to note that when the tag's size is small, it resonates at higher frequencies beyond the UHF spectrum. The fabrication process for the desired tag is simple and inexpensive. It involves depositing a 9  $\mu\text{m}$  thick double-sided layer of copper onto a flexible PET substrate with a thickness of 50  $\mu\text{m}$ . The tag's structure is created by etching away the unwanted copper layer, resulting in the PET substrate being wrapped symmetrically over the Styrofoam with a Ucode8 microchip embedded in a small narrow space along the meandered strip. The proposed tag can provide a directional radiation pattern when mounted on a substrate and embedded inside a metal cavity. A maximum impedance matching level of -34.33 dB is achieved with a read distance of up to 18.88 m when simulated inside the metal cavity or on metal surfaces. The resonant frequency and realized gain is are very stable with when different dimensions of the embedded cavity and depth are used. The physical prototype measurement has the same resonant frequency at 926 MHz with a maximum read distance of 12.32 m when embedded and 10.70 m when attached to the surface. Even though the measured read distance is slightly weaker than the simulated result, this is due to the TagFormance system being unable to calculate the

peak realized gain of the antenna at oblique angle  $37^\circ$  together with imperfection in the etching and fabrication process from human error.

Last but not least, by comparing the proposed antenna with other reviewed literature with directional radiation patterns, the proposed tag is among the most compact with tag's antenna structure is simple, with only  $30\text{ mm} \times 30\text{ mm} \times 5\text{ mm}$ , and yet can provide a long-read range distance of about 18.88m with close to 100% impedance matching and power transfer efficiency when embedded in metal cavity. As a result, the proposed antenna is highly versatile in tracking applications, as it can be embedded in or on metal without significantly affecting its performance.

## **5.2 Recommendations for Future Works**

The recommendations for future improvements include fabricating the antenna by using a proper copper etching machine from a third-party manufacturer. This is because the antenna etched using simple chemical etching may cause imperfection in human error and material error. For example, the defect during chemical etching, folding, and cutting of the antenna and defect in the copper material.

Next, other recommendations include implementing the embedded UCode8 microchip into the antenna using a proper fabrication machine from a third-party fabricator. Extracting the Ucode8 from commercial RFID tags and sticking it into the antenna feeding port causes imperfection and reduced impedance matching. Hence reducing the realized gain and read range during the measurement of the RFID antenna.

Besides, a low dielectric constant substrate must be used to alleviate high dielectric losses and cost saving, yet still maintain the compactness that needs to be explored to generate a smaller dimension and further read range antenna.

Lastly, the recommendation for future works is to use aluminium film instead of copper film for the antenna. This is because aluminium is far cheaper and more stable than copper, as copper is highly reactive to oxygen, forming a copper oxide that reduces the read range and impedance matching between the antenna and the microchip. Thus, making the antenna cheaper and easier to obtain a stable and repeatable performance.

## REFERENCES

- Bahr, W. and Price ,B. “Radio Frequency Identification and Its Application in E-Commerce”, *RFID Technologies and E-Commerce Process Improvement*, pp. 1-2. Retrieved from [https://publications.aston.ac.uk/id/eprint/28192/1/Radio\\_frequency\\_identification\\_and\\_its\\_application\\_in\\_e\\_commerce.pdf](https://publications.aston.ac.uk/id/eprint/28192/1/Radio_frequency_identification_and_its_application_in_e_commerce.pdf)
- Bansal, A., Sharma, S., and Khanna, R., 2019 "A Spiral Shaped Loop Fed high Read Range Compact Tag Antenna for UHF RFID Applications," *2019 IEEE International Conference on RFID Technology and Applications (RFID-TA)*, pp. 212-215. Retrieved from <https://ieeexplore.ieee.org/document/8892203>
- Chawla, V. and Ha, D. S., September 2007. "An overview of passive RFID," *IEEE Communications Magazine*, 45(9), pp. 11-17. Retrieved from [https://ieeexplore.ieee.org/abstract/document/4342873?casa\\_token=VC-DqgZpPSsAAAAA:W0nYVSi9B8jhipoTuQnLE-LyIH6b5Tjp8Kfun8gwKoRdhGgmiEyT71aAvTf81uDEz7G3Z7YZz8o](https://ieeexplore.ieee.org/abstract/document/4342873?casa_token=VC-DqgZpPSsAAAAA:W0nYVSi9B8jhipoTuQnLE-LyIH6b5Tjp8Kfun8gwKoRdhGgmiEyT71aAvTf81uDEz7G3Z7YZz8o)
- Chen, H. D. and. Tsao, Y. H., 2010. "Low-Profile Meandered Patch Antennas for RFID Tags Mountable on Metallic Objects," in *IEEE Antennas and Wireless Propagation Letters*, 9, pp. 118-121. Retrieved from <https://ieeexplore.ieee.org/document/5419020>
- George, B. A., David, F., G., Donald, C.K., Joseph, P., 1984. “Electro Magnetic Induction ”, *University Physics Academic Press* , pp. 650-666. Retrieved from <https://www.sciencedirect.com/science/article/pii/B9780120598601500394>
- Hamadeneg, S., Keskin, E., Aslshurideh, M., Masri, Y. and Al Kurdi, B., 2021. “The benefits and challenges of RFID technology implementation in supply chain: A case study from the Turkish construction sector” ,*Uncertain Supply Chain Management*. 9, pp. 1071-1080. Retrieved from [https://www.researchgate.net/publication/359352417\\_The\\_benefits\\_and\\_challenges\\_of\\_RFID\\_technology\\_implementation\\_in\\_supply\\_chain\\_A\\_case\\_study\\_from\\_the\\_Turkish\\_construction\\_sector](https://www.researchgate.net/publication/359352417_The_benefits_and_challenges_of_RFID_technology_implementation_in_supply_chain_A_case_study_from_the_Turkish_construction_sector)
- Landt, J., Oct.-Nov. 2005". The history of RFID," *IEEE Potentials*, 24(4), pp. 8-11, Retrieved from <https://ieeexplore.ieee.org/abstract/document/1549751>

- Lee, Y. H., Chee, P. S. Lim, E. H., and Bong, F. L., 2020. "Coupled-PILAs for Miniature On-metal RFID Tag Design," *2020 IEEE Asia-Pacific Microwave Conference (APMC)*, pp. 878-880. Retrieved from <https://ieeexplore.ieee.org/document/9331605>
- Lee, Y. H., Lim, E. H., Bong, F. L., Chung, B. K., Feb 2019. "Compact Folded C-Shaped Antenna for Metal-Mountable UHF RFID Applications", *IEEE TRANSACTIONS ON ANTENNAS AND PROPAGATION*, 67( 2), pp.765-773. Retrieved from <http://dx.doi.org/10.1109/TAP.2018.2879853>.
- Murofushi , R. H., and Tavares, J. J. P. Z. S. , April 2017. "Towards fourth industrial revolution impact: smart product based on RFID technology," in *IEEE Instrumentation & Measurement Magazine*, 20(2), pp. 51-56. Retrieved from [https://www.researchgate.net/publication/321386576\\_Introductory\\_Chapter\\_RFID\\_A\\_Successful\\_History](https://www.researchgate.net/publication/321386576_Introductory_Chapter_RFID_A_Successful_History)
- Ng, W.H., Lim, E. H., Bong, F.L., and Chung, B. K., June 2019. "Compact Planar Inverted-S Antenna With Embedded Tuning Arm for On-Metal UHF RFID Tag Design," in *IEEE Transactions on Antennas and Propagation*, 67, no. 6, pp. 4247-4252. Retrieved from <https://ieeexplore.ieee.org/document/8693903>
- White, G. R. T, Gardiner, G., Prabhakar, G., Razak, A. A., 2007. "A Comparison of Barcoding and RFID Technologies in Practice", *Journal of Information, Information Technology, and Organizations*, 2, pp. 121-122, Retrieved from [https://www.researchgate.net/publication/279650706\\_A\\_Comparison\\_of\\_Barcoding\\_and\\_RFID\\_Technologies\\_in\\_Practice](https://www.researchgate.net/publication/279650706_A_Comparison_of_Barcoding_and_RFID_Technologies_in_Practice)
- Xu, m., M, J. and Kim, S.H., 2018. "The Fourth Industrial Revolution: Opportunities and Challenges", *International Journal of Financial Research*, 9, pp. 90-95. Retrieved from: [http://creo.sc-celje.si/pluginfile.php/2387/mod\\_resource/content/1/4.1.4\\_01\\_The%20fourth%20industrial%20revolution.pdf](http://creo.sc-celje.si/pluginfile.php/2387/mod_resource/content/1/4.1.4_01_The%20fourth%20industrial%20revolution.pdf)
- Zhao, L., Ma, Y. and Meng, W., 2022. "M-Shaped Folded-patch Antenna for On-Metal UHF RFID Tag Design," *2022 IEEE International Conference on RFID (RFID)*, pp. 81-86. Retrieved from <https://ieeexplore.ieee.org/document/9795970>

## APPENDIX A

NXP Semiconductors

SL3S1205\_15

UCODE 8/8m

## 11 Characteristics

## 11.1 UCODE 8/8m bare die characteristics

Table 15. UCODE 8/8m RF interface characteristics (RF1, RF2)

Symbol	Parameter	Conditions	Min	Typ	Max	Unit	
$f_i$	input frequency		840	-	960	MHz	
$P_{i(min)}$	minimum input power	READ sensitivity	[1] [2] [3]	-	-22.9	-	dBm
		reduced operating range	[4]	-	+1	-	dBm
$P_{i(min)}$	minimum input power	WRITE sensitivity	[4]	-	-17.8	-	dBm
$t_{16bit}$	encoding speed	16-bit	[5]	-	0.7	-	ms
		32-bit (block write)	[5]	-	1.2	-	ms
$C_i$	chip input capacitance, Large Pads	parallel	[2] [6] [7]	-	0.69	-	pF
$Z$	chip impedance, Large Pads	866 MHz	[2] [6] [7]	-	15-j265	-	$\Omega$
		915 MHz	[2] [6] [7]	-	14-j252	-	$\Omega$
		953 MHz	[2] [6] [7]	-	13-j242	-	$\Omega$
$Z$	typical assembled impedance, Large Pads (see <a href="#">Figure 8</a> )	915 MHz	[8] [9] [7]	-	19-j234	-	$\Omega$
$Z$	typical assembled impedance in case of single-slit antenna assembly, Large Pads (see <a href="#">Figure 9</a> )	915 MHz	[8] [10] [7]	-	13-j191	-	$\Omega$

- [1] Power to process a QUERY command  
 [2] Measured with a 50  $\Omega$  source impedance directly on the chip  
 [3] Results in approximately -23 dBm tag sensitivity with a 2.15 dBi gain antenna  
 [4] Tag sensitivity on a 2.15 dBi gain antenna  
 [5] When the memory content is "0000...".  
 [6] At minimum operating power  
 [7] at center capacitor of Self Adjust  
 [8] The antenna shall be matched to this impedance  
 [9] Assuming 50ff additional assembly capacitance  
 [10] Assuming 220ff additional assembly+test pad capacitance

Table 16. UCODE 8/8m memory characteristics

Symbol	Parameter	Conditions	Min	Typ	Max	Unit
EEPROM characteristics						
$t_{ret}$	retention time	$T_{amb} \leq 55 \text{ }^\circ\text{C}$	20	-	-	year
$N_{endu(W)}$	write endurance		100k	-	-	cycle